X-RAY DIFFRACTION, PRINCIPLES AND APPLICATIONS

by

B. Buras

R. Fourme

and

M.H.J. Koch

X-RAY DIFFRACTION, PRINCIPLES AND APPLICATIONS

by

B. Buras
Physics Laboratory II, University of Copenhagen
Universitetsparken 5, DK 2100 Copenhagen, Denmark
and
Risø National Laboratory, DK-4000 Roskilde, Denmark

R. Fourme
L.U.R.E., Bâtiment 209c, Université Paris-Sud,
F-91405 Orsay-Cédex, France

M.H.J. Koch
European Molecular Biology Laboratory, c/o DESY,
Notkestrasse 85, D-2000 Hamburg 52, Fed. Rep. Germany

Running title: X-Ray Diffraction

Introduction

Introduction.

Although diffraction of X-rays has been observed
as early as 1908 by Walter and Pohl (1908a, 1908b)
it was really the presentation by Arnold
Sommerfeld of the work of W. Friedrich, P.
Knipping and M. von Laue (1912) on "X-ray
interference phenomena" at the meeting of the
Bavarian Academy of Sciences on June 8, 1912 which
initiated   X-ray diffraction as a major area of
research. This first publication was soon
followed by the papers of W.L. Bragg on the
"Diffraction of short electromagnetic waves by a
crystal " (Bragg, 1914) and by the first X-ray
study of the crystalline structure of copper
(Bragg, 1913). (A historical review of the
development of X-ray and neutron diffraction
supplemented by reprints of selected original
papers was published by Bacon (1966))
Seven decades have elapsed since then and the "gas
tubes" used as X-ray sources in the early days can
now only be found in museums. However, despite
considerable progress made on laboratory X-ray
sources- especially rotating anodes - in terms of
intensity and brightness, the qualitative features

of the radiation emitted by these sources has remained unchanged. The situation drastically changed in the last few years when the qualitatively and quantitatively very different synchrotron radiation (SR) X-ray sources became available.

The aim of the present chapter is to review briefly the new possibilities offered by SR sources for elastic scattering studies and to serve as an introduction to much of the material which will be presented in detail in the third volume of the Handbook.

The presentation is preceeded by a summary of the elementary theory of X-ray diffraction and a very brief description of the methods used. This introduction should help also non-diffractionists to fully appreciate the new developments. Diffractionists may only glance through this part except for the second section which is devoted to a general comparison of the possibilities offered by SR sources and conventional sources for diffraction studies. This part is followed by sections which review and illustrate the present status of elastic scattering research with SR. It should be stressed that we are only dealing with strictly elastic phenomena and hence, a number of

potential applications of SR concerning, for instance, weakly inelastic phenomena are not considered in this chapter. The last section gives an outlook on possible future applications.

1. Summary of the elementary theory of elastic X-ray scattering.

Only an elementary theory of elastic X-ray scattering is outlined below. Comprehensive and more advanced treatments can be found, for instance, in the books by Zachariasen (1967), James (1962), Warren (1969) and Azaroff et al.(1974). A slightly different approach was used by Marshall and Lovesey (1971) in the case of neutrons. It is the latter presentation which mostly influenced us and thus, the reader is referred to this book for detailed derivations of the formulae. Diffraction physics was recently also discussed by Feil (1977) and elastic scattering of X-rays by Stewart and Feil (1980). Scattering of X-rays (and neutrons) can also be described in terms of Van Hove's (1954) space and time correlation functions.

1.1 Interaction of X-rays with matter.

Being electromagnetic waves, X-rays interact with

electrons through electromagnetic forces. For our purpose their interaction with nuclei may be neglected as a result of the large inertial mass of the latter. [1]   In the present chapter we can consider that, to put it simply, X-rays "see" the electrons but not the nuclei.

Though known theoretically for a long time, the interaction of X-rays with magnetic moments was only very recently demonstrated experimentally. The group of Erwin Bertaut at Grenoble (de Bergevin and Brunel, 1972) detected an interaction between X-rays and the magnetic moment of an atom, which, although very weak,can be used for magnetic scattering experiments, especially when very intense SR sources are used. (see 3.1.5.2.)
In the range of photon energies below 1 MeV two processes should be considered in the interaction of X-rays with matter: scattering which can be either elastic or inelastic, and absorption.
Elastic scattering occurs when the photon energy and thus also the internal energy of the scatterer remain unchanged. Conversely in inelastic

---

[1]   Note that photons in the γ-region can be a powerful tool to explore the nuclear structure. The potential of SR in this area have recently been discussed by Molinari (1980).

scattering the photon energy and hence also the internal energy of the scatterer change, as for instance, in Compton scattering, in which a part of the photon energy is transferred to one particular electron, or in scattering by elementary excitations in solids or liquids (e.g. phonons, plasmons).

The present chapter deals with elastic scattering only. However, it should be kept in mind that in every elastic scattering experiment, the possibility of having inelastic processes and/or absorption must be considered and- if necessary- appropriate corrections should be made. This applies, in particular, to thermal diffused scattering (TDS) which is usually peaked below the Bragg peak.

1.2. The scattering geometry; scattering cross-section and scattering amplitude for a free electron.

The geometry of the scattering problem is illustrated in figure 1. The incident single photon can be represented by a plane wave:

$$\psi_i = \exp(i \cdot \vec{k}_i \cdot \vec{r}) \qquad (1)$$

where $\vec{k}_i = 2\pi/\lambda_i$ is the incident photon wave vector and λ_i is the wavelength of the incident X-rays. As shown by Thomson (1933) the wave scattered per unit time by a free electron at sufficiently large distances r from the electron is given by:

$$\psi_j = -\frac{e^2}{mc^2} \frac{1}{r} \exp(i \vec{k}_j \cdot \vec{r}) \sin\chi$$

$$= -\frac{r_o}{r} \exp(i \vec{k}_j \cdot \vec{r})(\vec{E}_i \cdot \vec{E}_j) \qquad (2)$$

where $r_o = e^2/mc^2$ is the classical electron radius, k_j is the scattered wave vector, χ the angle between the direction of travel of the scattered beam and the electric vector of the incident plane polarized X-ray beam. $\vec{E}_i$ and $\vec{E}_j$ are the polarization vectors of the incident and scattered beam, respectively. For elastic scattering:

$$\vec{k}_i = \vec{k}_j \qquad (3)$$

The scattering amplitude is $(-r_o)$ and $\sin\chi = \vec{E}_i \cdot \vec{E}_j$ is the polarization factor. The negative sign indicates that a phase shift of $180°$ occurs in the scattering process.

The differential scattering cross-section is defined as the ratio of the number of photons (dn) scattered by a single electron into a solid angle (dΩ) to the photon flux (ϕ):

$$\frac{d\sigma}{d\Omega} = \frac{dn/d\Omega}{\phi} \qquad (4)$$

The photon flux ϕ is the number of photons passing perpendicularly through a unit area in a unit time (e.g. 10^9 photons/cm^2 s). For a plane polarized incident X-ray beam scattered by a free electron the differential scattering cross-section is given by:

$$\frac{d\sigma}{d\Omega} = r_0^2 \sin^2\chi = r_0^2 \left(\vec{E_i} \cdot \vec{e_f} \right)^2 \qquad (5)$$

whereas for an unpolarized incident X-ray beam, as is usually the case when characteristic radiation from a conventional source is used, the polarization factor has to be averaged over all possible values of χ . In this case the differential cross section is given by:

$$\frac{d\sigma}{d\Omega} = r_0^2 \left(\frac{1 + \cos^2 2\theta}{2} \right) \qquad (6)$$

where 2θ is the scattering angle as defined in figure 1. (Some authors e.g. Marshall and Lovesey (1971) denote the scattering angle by θ) In the case of SR, X-rays are to a large degree polarized in the plane of the electron orbit. The component perpendicular to the electron orbit plane can, however, usually not be neglected. Thus the polarization factor must be carefully calculated or measured in each case, taking into account not only the polarization of the primary SR beam but also the polarization caused by the optical elements e.g. mirrors , monochromators and analyzers. An example is given by Phillips et al. (1977) for a precession camera, in a paper which also contains references to the earlier literature on polarization factors.

1.3. Scattering by an atom; Atomic scattering factor.

The scattering amplitude A_a for a collection of electrons in an atom is the sum of the scattering amplitudes of all electrons taking into account the phase differences arising from the spatial

distribution of the electrons which are assumed to be free.

This assumption is verified for photon energies much higher than the binding energy of the innermost shell whereas for lower photon energies the bound character of the atomic electrons becomes noticable as discussed in 1.4.

The phase differences can be calculated as indicated in figure 2. The path difference which is equal to (OA-BM) results in a phase difference ϕ of $2\pi (OA-BM)/\lambda_i$. Hence,

$$\phi = \vec{\varkappa} \cdot \vec{r} \qquad (7)$$

where

$$\vec{\varkappa} = \vec{k}_f - \vec{k}_i \qquad (8)$$

is called the scattering vector. Multiplication of Eq. (8) by $\hbar$ (i.e. the Planck constant divided by 2π) gives:

$$\hbar\vec{\varkappa} = \hbar\vec{k}_f - \hbar\vec{k}_i \qquad (9)$$

which expresses the law of momentum conservation as illustrated in figure 3 by the isosceles momentum triangle ($\hbar$ is omitted in this figure). $\hbar\vec{\varkappa}$ is thus the momentum transferred by the electron to the photon. $\hbar\vec{\varkappa}$ and frequently- when it is not causing confusion - $\vec{\varkappa}$ itself is called momentum transfer, the two names of $\vec{\varkappa}$, scattering vector and momentum transfer, being used interchangeably. The modulus of the scattering vector, as calculated from figure 3, equals:

$$\varkappa = 2 k \sin\theta = 4\pi \frac{\sin\theta}{\lambda} = 4\pi \frac{E \sin\theta}{hc} \qquad (10)$$

where c is the velocity of light and E the photon energy. hc is approximately equal to 12.4 keV Å and thus:

$$\varkappa \simeq E \sin\theta \qquad (11)$$

if E is expressed in keV and $\varkappa$ in Å^{-1}. Taking Eq.7 into account one obtains the scattering amplitude of an atom:

$$A_a(\vec{\varkappa}) = -r_0 (\vec{\varepsilon}_i \cdot \vec{\varepsilon}_f) \sum_{j=1}^{z} \exp(i\vec{\varkappa} \cdot \vec{r}_j) \qquad (12)$$

where $\vec{r_j}$ is the position vector of the j-th electron and Z is the atomic number. Introducing the electron density function $\rho(\vec{r})$, such that $\int \rho(\vec{r})dv$ is the number of electrons in the volume element dv one obtains:

$$A_a(\vec{\varkappa}) = -r_o(\vec{\mathcal{E}_i}\cdot\vec{\mathcal{E}_f}) \int \rho(\vec{r}) \exp(i\vec{\varkappa}\cdot\vec{r}) \, dv \quad (13)$$

The integration is over the atomic volume.
In crystallography, the atomic scattering factor is defined as:

$$f(\varkappa) = \frac{A_a(\vec{\varkappa})}{-r_o(\vec{\mathcal{E}_i}\cdot\vec{\mathcal{E}_f})} = \int \rho(\vec{r}) \exp(i\vec{\varkappa}\cdot\vec{r}) \, dv \quad (14)$$

As can be seen, $f(\vec{\varkappa})$ depends only on the electron density distribution. Since $\rho(\vec{r})$ and $f(\vec{\varkappa})$ are related by a Fourier transformation, both functions are equivalent descriptions of an assembly of electrons in an atom: $\rho(\vec{r})$ in real space and $f(\vec{\varkappa})$ in momentum space. It can already be seen from Eq. 14 that large distances r in real space correspond to small $\varkappa$ in momentum

space. This relationship and the momentum space are discussed in some detail in 1.5. with the example of the reciprocal lattice.

Figure 4 illustrates the dependence of the atomic scattering factor on the modulus of the scattering vector for Calcium (Z=20) and Zirconium (Z=40) atoms as calculated from the electron density distributions obtained from the Thomas-Fermi-Dirac statistical model (International Tables for X-ray Crystallography, 1962).

It is clear from this figure that the atomic scattering factor

a) is equal to the atomic number Z for forward scattering ($\varkappa$ =0)

b) is, especially for small scattering vectors, a rapidly decreasing function of $\vec{\varkappa}$.

c) decreases more slowly with $\vec{\varkappa}$ for atoms with higher Z.

1.4. Anomalous scattering

As already mentioned earlier at photon energies close to the binding energy of the innermost shells, an atom can no longer be considered as an assembly of free electrons and the equations given

above have to be modified (see e.g. Anomalous scattering (1975) and Wendin (1980) and references therein). In this elementary introduction, we use the classical theory of dispersion which supposes that the atoms scatter electromagnetic waves as if they consisted of electric dipole oscillators having certain definite natural frequencies. It can be shown that the scattering amplitude from such an oscillator is given by:

$$A = -\kappa_o \left(\vec{\epsilon_i} \cdot \vec{\epsilon_f} \right) \frac{\omega^2}{\omega^2 - \omega_s^2 - i f \omega} \quad (15)$$

where it is assumed that the incident electromagnetic wave has a unit amplitude (cfr Eq.1) and where ω_s is the natural frequency of the oscillator; $\omega = c k$ is the frequency of the incident radiation and f is the damping factor. Thus the scattering factor f_e for a dipole oscillator is:

$$f_e = \frac{\omega^2}{\omega^2 - \omega_s^2 - i f \omega} \quad (16)$$

For a free electron ($\omega_s = 0$ and $f = 0$) one obtains, as expected, $f_e = 1$. Eq. 16 can also be rewritten in the following form:

$$f_e = 1 + f_e' + i f_e'' \quad (17)$$

which shows that the scattering factor for a dipole oscillator can be considered as the sum of the structure factor of a free electron, a real term f_e' and an imaginary term f_e'' . Similarly, the atomic scattering factor can be in general expressed as:

$$f = f_o + f' + i f'' \quad (18)$$

where f_o is the structure factor for photon energies much higher than the binding energy of the innermost shell ($\omega \gg \omega_s$) discussed in section 1.3 and f' and f'' are the real and imaginary part of the contribution caused by the presence in the atom of a natural frequency ω_s close to the incident photon frequency ω. The

two dispersion corrections are related by the Kramers-Kronig relationship (Kronig and Kramer, 1928):

$$f'(\omega) = \frac{e}{\pi} \int_0^{\infty} \frac{\omega' f''(\omega')}{\omega^2 - \omega'^2} \, d\omega' \qquad (19)$$

In practice, it suffices to integrate over a suitable finite range of frequencies to obtain reliable values of f', given the wavelength dependence of f". The latter is directly related to the wavelength dependence of the linear absorbtion coefficient $\mu(\omega)$:

$$f''(\omega) = \frac{m\omega}{4\pi e^2} \frac{A}{N} \cdot \mu(\omega) \qquad (20)$$

where N is Avogadro's number and A is the atomic weight. The study of the correlated behaviour of f' and f" is of special interest for elements which exhibit so-called white lines in their absorption spectra (see e.g. Lye et al., 1980, and references therein, Templeton et al. 1980a, Templeton et al. 1980b). f' and f" display exceptionally large variations over the very narrow wavelength range of the white line. The

dependence of f' and f" on the wavelength is illustrated in figure 5 for Caesium. The values of the real and imaginary part of the atomic scattering factor can be obtained from various kinds of measurements which are briefly discussed in section 3.1.3.2. It should be noted that contrary to the values of f , the values of f' and f" are not very dependent on the angle so that at large momentum transfers the contribution of the dispersion terms becomes relatively more important. Applications of anomalous scattering to structural problems are discussed in 3.1.3.1.

1.5 Scattering from a crystal. Structure factor.

Elastic scattering from crystals is best understood in terms of the reciprocal lattice, which is a momentum space. The brief reminder of the reciprocal lattice given below gives an opportunity to become familiar with the concept of momentum space - an indispensable prerequisite for the understanding of all scattering phenomena.

1.5.1 The reciprocal lattice

The unit vectors of the elementary cell in real space are denoted by $\vec{a_1}, \vec{a_2}, \vec{a_3}$, and the volume of the unit cell in real space is $N_o = \vec{a_1} \cdot (\vec{a_2} \times \vec{a_3})$. The lattice vector leading from a point in one unit cell to a corresponding point in another cell is denoted by $\vec{p}$, and

$$p = p_1 \vec{a_1} + p_2 \vec{a_2} + p_3 \vec{a_3} \qquad (21)$$

where p_1 , p_2 , p_3 are integers. By translation of the elementary cell using this lattice vector one obtains the crystal lattice in real space, in which any set of crystallographic planes is characterized by the Miller indices h, k, l, which are integers without common factor.

The reciprocal elementary cell is defined by the reciprocal unit vectors $\vec{a_1^*}$, $\vec{a_2^*}$, $\vec{a_3^*}$ (physicists frequently denote these vectors by $\vec{\tau_1}$, $\vec{\tau_2}$ and $\vec{\tau_3}$) related to the unit vectors of the elementary cell in real space by the following relations :

$$\vec{a_i} \cdot \vec{a_k^*} = \begin{cases} 2\pi & \text{if } j = k \\ 0 & \text{if } j \neq k \end{cases} \qquad (22)$$

These equations can be satisfied by choosing

$$\vec{a_1^*} = 2\pi \frac{\vec{a_2} \times \vec{a_3}}{N_o} \;;\; \vec{a_2^*} = 2\pi \frac{\vec{a_3} \times \vec{a_1}}{N_o} \;;\; \vec{a_3^*} = 2\pi \frac{\vec{a_1} \times \vec{a_2}}{N_o}$$

Crystallographers usually omit the factor 2π, whereas most solid state physicists include it. By analogy with the lattice vector, a reciprocal lattice vector is defined as

$$\vec{\lambda}_{HKL} = H\vec{a_1^*} + K\vec{a_2^*} + L\vec{a_3^*} \qquad (23)$$

where H, K and L are integers. By translating the reciprocal elementary cell using this vector, one obtains the reciprocal lattice. The relation between the crystal lattice in real space and the reciprocal crystal lattice is illustrated in figure 6 for the two dimensional case. As can be seen, a set of crystallographic planes (hkl) in real space is represented in the reciprocal lattice by a point h, k, l given by the reciprocal lattice vector

$$\vec{\lambda}_{hkl} = h\vec{a_1^*} + k\vec{a_2^*} + l\vec{a_3^*} \qquad (24)$$

perpendicular to the set of crystallographic planes (hkl) in real space (physicists denote the reciprocal lattice vector by $\vec{\tau}$; $\vec{H}$ and $\vec{G}$ are also in common use). Its modulus is

$$\left| \vec{\mathcal{S}}_{hkl} \right| \;=\; \mathcal{S}_{hkl} \;=\; \frac{2\pi}{d_{hkl}} \qquad (25)$$

where d_{hkl} is the interplanar spacing of the (hkl) crystallographic planes. It should be noted that a reciprocal lattice point HKL, where

$$H = nh \;, \qquad K = nk \;, \qquad L = n\ell$$

with n as an integer larger than 1 does not correspond to any set of <u>crystallographic</u> planes in real space. It corresponds, however, as can be shown, to <u>geometrical</u> planes in real space, parallel to the (hkl) planes and separated by d_{hkl}/n. The physical meaning of these reciprocal lattice points will be come clear when discussing diffraction. Note that for any $\vec{p}$

$$\vec{\mathcal{S}} \cdot \vec{p} = 2\pi \left(H p_1 + K p_2 + L p_3 \right) = 2\pi \times integer \quad (26)$$

and thus

$$exp\left(i\, \vec{\mathcal{S}} \cdot \vec{p} \right) \;=\; 1 \qquad (27)$$

1.5.2 Scattering from a crystal. Structure factor. Total scattering cross-section.

The simplest crystal corresponds to a Bravais lattice (one atom per unit cell). In this case the lattice vectors $\vec{p}_j$, where j numbers the unit cells, give the positions of the atoms, and the scattering amplitude of the crystal is given by:

$$A(\vec{\varkappa}) = \sum_{j=1}^{N} A_a(\vec{\varkappa}) \; exp\left(i\, \vec{\varkappa} \cdot \vec{p}_j \right)$$

$$= -\varkappa_0 \, f(\vec{\varkappa}) \left(\vec{E}_i \cdot \vec{E}_f \right) \sum_{j=1}^{N} exp\left(i\, \vec{\varkappa} \cdot \vec{p}_j \right) \qquad (28)$$

where it was taken into account that all atoms are identical and N is the number of unit cells. The differential scattering cross-section is:

$$\frac{d\sigma}{d\Omega} = \varkappa_0^2 \, \left| f(\vec{\varkappa}) \right|^2 \left(\vec{E}_i \cdot \vec{E}_f \right)^2 \left| \sum_{j=1}^{N} exp\left(i\, \vec{\varkappa} \cdot \vec{p}_j \right) \right|^2 \quad (29)$$

As indicated in eq. 27, $\exp(i\,\vec{s}\cdot\vec{p_j}) = 1$ for all j. Hence, if $\vec{K}$ is equal to zero or to any reciprocal lattice vector $\vec{s}$, the differential scattering cross-section, $\frac{d\sigma}{d\Omega}$ is large since all terms in the sum add up in phase. However, as $\vec{K}$ moves away from a reciprocal lattice vector, the terms in the sum rapidly get out of phase and the right-hand side of Eq. 29 decreases to a negligible value. Thus, for each reciprocal lattice vector, the scattering cross-section behaves as a Dirac delta function and hence, for a large crystal, the scattering cross-section can be expressed as a sum of Dirac delta functions (δ), each representing the contribution from one reciprocal lattice point. It can be shown that for a Bravais lattice

$$\frac{d\sigma}{d\Omega} = r_o^2\ \frac{(2\pi)^3}{N_o}\ \sum_{\vec{s}}\ |f(\vec{s})|^2\ \delta(\vec{K}-\vec{s})\cdot(\vec{E_i}\cdot\vec{E_j})^2 \quad (30)$$

The atomic scattering factor $f(\vec{s})$ and the polarization factor $(\vec{E_i}\cdot\vec{E_j})$ which, in the case of X-rays) depend on s have to be summed over $\vec{s}$. For a non-Bravais lattice, the positions of the N_o atoms in the unit cell in real space are given

by:

$$\vec{K}_m = x_m\ \vec{a_1} + y_m\ \vec{a_2} + z_m\ \vec{a_3} \quad (31)$$

where $m = 1,2 \ldots\ldots N_o$ numbers the atoms. Note that x_m, y_m, z_m are coordinates expressed in fractions of the unit cell vectors, i.e.

$$0 \le x_m \le 1\ ;\quad 0 \le y_m \le 1\ ;\quad 0 \le z_m \le 1$$

Eq. 30 can be generalised to a non-Bravais lattice by introducing the unit cell structure factor. In the static case, i.e. when thermal vibration can be neglected, one obtains the following formula for the differential scattering cross section for a non-absorbing crystal of volume V:

$$\frac{d\sigma}{d\Omega} = \frac{(2\pi)^3}{N_o^2}\cdot V\cdot r_o^2 \sum_{\vec{s}}\ \delta(\vec{K}-\vec{s})\ |F(\vec{s})|^2(\vec{E_i}\cdot\vec{E_j})^2 \quad (32)$$

and for the total scattering cross-section:

$$\sigma_t = \frac{(2\pi)^3}{N_o^2}\ V\cdot r_o^2\ |F(\vec{s})|^2\ \delta(s^2 - 2k_i\cdot s\sin\theta)(\vec{E_i}\cdot\vec{E_j})^2 \quad (33)$$

where

$$F(\vec{s}') = \sum_{m=1}^{N_o} f_m(\vec{s}') \ exp(i \ \vec{s}' \cdot \vec{r}_m) \qquad (34)$$

is the <u>unit cell structure factor.</u>

It follows from the definitions of $\vec{s}'$ and $\vec{r}_m$ and from Eq. 22 that

$$\vec{s}' \cdot \vec{r}_m = 2\pi \left(H x_m + K y_m + L z_m \right) \qquad (35)$$

and thus

$$F(\vec{s}) = \sum_{m=1}^{N_o} f_m(\vec{s}) \ exp \left[2\pi i \left(H x_m + K y_m + L z_m \right) \right] \qquad (36)$$

As already indicated earlier, this formula is only valid for a static lattice. In the general case, however, thermal vibration which smears out the electron density, thereby decreasing the atomic scattering amplitude and thus also the atomic structure factor, cannot be neglected. Thermal effects are taken into account by introducing the temperature factor $exp(-W_m(\vec{s}))$ into eq. 36 which yields:

$$F(\vec{s}) = \sum_{m=1}^{N_o} f_m(\vec{s}) \ exp\left(-W_m(\vec{s})\right) \ exp\left[(2\pi i \left(H x_m + K y_m + L z_m \right)\right] \qquad (37)$$

In the simple case of harmonic thermal vibration $W_m(\vec{s})$ is given by:

$$W_m(\vec{s}) = \frac{1}{2} s^2 < x^2 >_m \qquad (38)$$

where $< x^2 >_m$ is the mean square displacement of the m-th atom in the direction of $\vec{s}$. More complicated formulae are required to treat the case of anharmonic thermal motion.

In more general terms we can consider the unit cell to have a continuous electron density distribution, instead of discrete individual atoms, and if $\rho(\vec{r})$ denotes the electron density distribution function, $F(\vec{s})$ can be defined - as it was done for an atom - as

$$F(\vec{s}) = \int \rho(\vec{r}) \ exp(i \ \vec{s} \cdot \vec{r}) \, dv \qquad (39)$$

where the integration is over the unit cell. Clearly, the unit cell structure factor is the Fourier transform of the electron density distribution function $\rho(\vec{r})$ and vice versa $\rho(\vec{r})$ is the Fourier transform of $F(\vec{s})$. Thus the unit cell structure factor is the key quantity to be measured in order to determine the crystal structure.

It follows from Eq. 32 and 33 that a necessary condition for a term in the sum to be non-zero is that $\vec{\mathcal{K}} = \vec{s}$ or in the scalar form, $\Delta = 2\,k_i\sin\theta$. This is Bragg's law applied to the scattering cross-section as illustrated in Fig. 7 by the well-known Ewald construction in the reciprocal lattice. As can be seen from this figure, the Ewald circle (or sphere in three dimensions) may cross several reciprocal points (e.g. HKL and H'K'L'). Thus the Bragg condition may be fulfilled for several scattering angles and in this case one observes several reflections, each in a different direction. Figure 8 explains, as an example, the diffraction of a white collimated beam by a single crystal, in terms of the reciprocal lattice. For reasons of clarity the Ewald circles are omitted and only the isosceles triangles illustrating the momentum conservation

law are shown for the 111, 222, 333.... reflections. These higher order reflections contained in the diffracted beam cause problems in the design of single crystal monochromators. (see chapter 4)

It should be remembered, in connection with the Ewald construction, that $\hbar\vec{\mathcal{K}}$ is the momentum transferred (in this case by the periodic lattice) to the photon and thus $\hbar\vec{s}$ also represents a momentum. Thus the reciprocal lattice is a three-dimensional momentum space with unit vectors $\hbar\vec{a}_1^*, \hbar\vec{a}_2^*, \hbar\vec{a}_3^*$ and the reciprocal lattice points represent a discrete set of momenta which can be transferred to a photon to change its direction of propagation without change in its energy (elastic scattering).

It is clear from figure 8 and from the discussion at the end of 1.5.1 that the lattice points with

$$H = nh \qquad K = nk \qquad L = nl$$

where (hkl) are the Miller indices and n is an integer, correspond to the nth-order reflection from the hkl crystallographic plane, which can be interpreted as a first order reflection from planes separated by d_{hkl}/n.

It follows from the above that, as already mentioned, small distances in real space correspond to large momenta in momentum space and vice versa. This can be generalised to any scattering e.g. from atoms, liquids, amorphous substances, etc.

Obviously, a non-zero structure factor $F(\vec{s})$ is another necessary condition to have a non-zero term in the sum in Eqs. 32 and 33.

From Eq. 33 one can see that the total scattering cross-section is the sum of scattering cross-section $\sigma(\vec{s})$ for the particular reflections specified by the reciprocal vector $\vec{s}$:

$$\sigma(\vec{s}) = \frac{(2\pi)^3}{N_0^2} V \cdot r_0^2 \frac{2}{\hbar_i} |F(\vec{s})|^2 \delta(s^2 - 2\hbar_i s \sin\theta)(\vec{\xi}_i \cdot \vec{\xi}_f)^2 \quad (40)$$

In an experiment aimed at the determination of a crystal structure one first has to find a number of reflections, depending on the complexity of the structure. Secondly, one must find the unit cell structure factors corresponding to these reflections by measuring the integrated intensities as described in section 1.5.4.

1.5.3 Angular analysis and energy analysis

Since reflections will only occur if the Bragg condition $\vec{\varkappa} = \vec{s}$ is fulfilled one must be able to change both the direction of $\vec{\varkappa}$ relative to the reciprocal lattice and its magnitude. For the most frequent case i.e. where the direction of $\vec{k}_i$ is fixed, the direction of $\vec{\varkappa}$ relative to the sample can be changed by reorienting the sample. For isotropic samples, e.g. powdered crystals, liquids, amorphous substances, this is obviously not necessary.

There are two principal methods to vary the magnitude of $\varkappa$ as can be seen from Eq. 10. In the first method, which is usually called angular analysis or angular dispersive method, one measures the angular distribution of the diffracted radiation using a monochromatic incident beam (fixed $\hbar_i$ and ξ_i) and varies the scattering angle. The second approach called energy analysis or energy dispersive method uses a polychromatic ("white") incident beam at a fixed scattering angle and measures the wavelength (photon energy) distribution of the diffracted radiation. Figure 9 illustrates the example of

the diffraction pattern of powdered $BaTiO_3$ obtained by the two types of methods.

The experimental details of both types of methods are beyond the scope of this review, but a schematic representation of the various approaches is given in Table 1. Some comments concerning the less known white beam methods are made in section 2.6. The polychromatic powder method utilizing synchrotron radiation was recently reviewed by Buras (1980) and the polychromatic single crystal methods are discussed by Buras et al. (1980a). Laine and Lahteenmaki (1980) published an annotated bibliography for the period 1968-1978 of the energy dispersive X-ray diffraction method. For details concerning the monochromatic beam methods see International Tables for X-ray Crystallography (1962) and references therein.

1.5.4 Integrated intensity

According to Eq. 33 each reflection should be a δ-function, but in practice the peak has a non zero width determined in each of the methods listed in Table 1, by other factors: spectral

width of the incident beam in the monochromatic methods, energy resolution of the solid state detector in the white beam methods, collimation, mosaic spread in the case of single crystals etc. The area under the peak, after background subtraction, as defined in figure 10, is called the integrated intensity. For the monochromatic beam methods integration is over the angle, for the white beam methods over the wavelength. In the case of a single crystal and a white beam

$$P(\vec{s}') = \int i_o(\lambda)\, \sigma_t\, (\vec{s}')\, d\lambda =$$

$$= i_o(\lambda_B)\, \frac{V}{v_o^2}\, \frac{\lambda_B^4\, |F(\vec{s}')|^2}{\sin^2\theta_B}\cdot (\vec{\varepsilon_i}\cdot\vec{\varepsilon_j})^2 \quad (41)$$

where $i_o(\lambda)$ is the incident intensity per unit wavelength, $\sigma_t(\vec{s})$ is the total elastic scattering cross-section given by Eq. 33 and λ_B and θ_B correspond to the Bragg condition.

In the case of a single crystal, rotated through the reflection range, and a monochromatic beam of wavelength λ_o

$$P(\vec{s}) = \int i_o(\lambda_o)\, \Delta\lambda_o\, \sigma_t\, (\vec{s})\, d\theta$$

$$= I_o\, \frac{V}{v_o^2}\, \frac{\lambda_o^3\, |F(\vec{s})|^2}{2\pi\, \sin 2\theta_B}\, (\vec{\varepsilon_i}\cdot\vec{\varepsilon_j})^2 \quad (42)$$

where $\Delta\lambda_o$ is the wavelength spread of the incident monochromatic beam, defined in the case of SR by the collimation of the white beam incident on the monochromator and the properties of the latter. (see Chapter 4) Thus $I_o = i_o(\lambda_o)\Delta\lambda_o$ is the intensity of the incident monochromatic beam.

Formulae for the integrated intensities for all methods listed in Table 1 are presented in Table 2 (Buras and Gerward, 1975). The formulae for powders correspond to the whole Debye-Scherrer ring and those for rotating single crystals are for a full rotation around a zone axis. j' denotes the multiplicity factor for powders and j" is the number of equivalent reflections in the zone under study. p is $(\vec{\mathcal{E}}_i \cdot \vec{\mathcal{E}}_f)^2$ and $\Delta\theta_o$ the overall spread of the incident and diffracted beams defined by the collimation system.

Details concerning formulae for integrated intensities for the monochromatic beam methods can be found in International Tables for X-Ray Crystallography Vol. 2 (1962). As far as white beam methods and relations between the various formulae listed in Table 2, are concerned the reader is referred to Buras and Gerward (1975) and references therein as well as to a recent paper by Kalman (1979).

All formulae presented in Table 2 were derived in the kinematic approximation in which the interaction between the direct and reflected beams is neglected. The dynamical theory of diffraction which takes this interaction into account is beyond the scope of this elementary introduction. The formulae in Table 2 are given for non-absorbing samples whereas the quantity measured is:

$$P_{meas}(\vec{\lambda}) = P(\vec{\lambda}) \cdot A \qquad (43)$$

where A is the measured absorption factor which for a simple transmission geometry given by

$$A = exp\left(-\mu(\lambda)\cdot x\right) \cdot exp\left(-\mu_1(\lambda)\cdot x_1\right) \qquad (44)$$

where $\mu(\lambda)$ and $\mu_1(\lambda)$ are the linear absorption coefficients of the sample and the surrounding medium respectively, and x and x_1 are the paths of the beam in the sample and the surrounding medium, respectively. When the beam paths are of varying

length within the sample one has to integrate
(usually numerically) over the irradiated volume
in order to find the absorption factor. For
windows etc. other terms should be included in
Eq. 44. In the case of a monochromatic beam
$\mu(\lambda)$ = constant and the other terms in Eq. 44
are, in general, also constant. In the case of a
polychromatic beam, both $\mu(\lambda)$ and $\mu_{1}(\lambda)$ are
wavelength dependent and thus both terms should be
taken into account.

2. Diffraction studies with X-rays from
conventional sources and from synchrotron
radiation sources

2.1 Phase problem

As mentionned before (1.5.2), the crucial
quantity in structural studies is the unit cell
structure factor $F(\vec{s})$. In general it is a complex
number which can be expressed as

$$| F(\vec{\lambda})| \, exp \, (i \, \phi) \qquad (45)$$

where $|F(\vec{\lambda})|$ is the modulus and ϕ is the phase.
In order to perform a Fourier transform one must
know both the modulus and the phase. As can be
seen from Eqs. 41 and 42 and Table II, the
measurement of integrated intensities, however,
give only the modulus of the structure factor but
not its phase. This creates the so-called "phase
problem". Various sophisticated techniques have
been developed to get round this problem. One of

the methods is based on anomalous scattering (see 1.4) and will be discussed in (3.3.1.) The method relies on the dependence of the atomic scattering factor (and its phase) on the wavelength, as indicated in figure 5, and thus requires a source with a continuous spectrum from which any wavelength can be selected. The continuous Bremsstrahlung even from rotating anode sources is not sufficiently intense to perform these measurements whereas it has already been shown (see section 3.3.1) that it is possible to determine phases using SR.

2.2 Large scattering vectors

In any case, in order to obtain an accurate Fourier transform (electron density distribution) it is necessary to measure $F(\vec{s})$ in a large range of $\vec{\mathcal{K}}$. In particular, if one is interested in the structure at short distances in real space, one must use data corresponding to large scattering vectors. $\mathcal{K}$ can be made large by increasing the scattering angle (see Eq. 10) but even for backscattering ($2\theta = 180°$):

$$\mathcal{K}_{max} \simeq \frac{4\pi}{\lambda_i} \sim E_i \qquad (46)$$

The short wavelength radiation obtained from X-ray tubes is usually the MoK$_\alpha$ radiation with $\lambda = 0.711$ Å (17.44 keV) and $\mathcal{K}_{max} = 17$ Å^{-1}. The useful radiation from a synchrotron source extends to about $1/5\lambda_c$ ($5E_c$) and thus $\mathcal{K} = 17\text{Å}^{-1}$ can be obtained even with a storage ring with a rather long critical wavelength, e.g. $\lambda_c = 3.5$ Å ($E_c = 3.5$ keV). Larger values of $\mathcal{K}$ can be obtained (also at scattering angles smaller than 180°) from storage rings with smaller λ_c (larger E_c) and/or from wigglers(which shift the whole spectrum towards shorter wavelengths) installed on a low energy machine.

It is clear from Table 3 in Chapter 1 that with the available storage rings, but more so with the machines under construction, one has the possibility of measuring structure factors in a much wider range than can be done with conventional sources. This offers a unique possibility for more accurate structure determination.

2.3 Small scattering vectors

If one is interested in the structural features corresponding to large distances in real space, one must measure the structure factors corresponding to small scattering vectors. Because of strong absorption at very long wavelength (low photon energy) the obvious way of obtaining measurements at small $\mathcal{K}$-values is to decrease the scattering angle. This is the basis of the small angle scattering techniques discussed in more detail in section 4.

For this type of measurements the excellent collimation and high intensity of SR are of great advantage. These two features enable to place the detector far from the sample and close to the direct beam which permits high resolution measurements at very small angles.

2.4 Small samples

As shown in Table II the integrated intensity is directly proportional to the product of the incident intensity and sample volume in the monochromatic beam methods and to the product of incident intensity per unit wavelength and sample

volume in the white beam methods. Thus the more intense and brighter the source, the s   the sample can be for the same measured si   '. This is especially important in cases where only minute samples can be used (e.g. very small biological single crystals, powders in diamond anvil high pressure cells, thin films either freely suspended or on a surface).

The gain arising from the high intensity of SR sources as compared with conventional sources is obviously larger for white beam methods than for monochromatic beam methods. There is still, however, a large gain for monochromatic beam methods which might dramatically increase when undulators for the X-ray region become available.

2.5. Resolution

As discussed in detail in Chapters 3 and 4, a monochromatic beam of any wavelength can be selected from the continuous SR spectrum. In addition to this tunability, a large variety of monochromators enables one to tailor the beam to the experiment, both regarding monochromaticity

and collimation in a wide range of $\Delta\lambda$ and $\Delta\vec{k}_i$. The small $\Delta\lambda$ and $\Delta\vec{k}_i$ are especially important for high resolution measurements. This favourable situation results from the excellent intrinsic collimation of SR and its high intensity, part of which can be sacrificed in favour of resolution.

2.6 White beam diffractometry

As already mentioned under 2.3, white radiation from SR sources is much more intense than Bremsstrahlung from conventional sources. Other advantages of SR, for white beam methods, as compared with conventional sources, are (Buras, 1980):

(a) a smooth and continuous spectrum without characteristic lines.

(b) a spectrum which extends to larger photon energies than in the case of conventional sources.

(c) a spectrum which can be calculated. This is especially important for the white beam methods which require the knowledge of the incident spectrum $i_o(\lambda)$ for structure factor calculations.

(d) a polarisation which dependence on photon

energy can be calculated.

(e) a highly collimated incident beam.

(f) a high intensity which can be traded off against resolution.

2.7 Samples with large unit cells.

It follows from Table II that in all methods the integrated intensity is inversely proportional to the square of the unit cell volume in real space. Thus crystals with large unit cells give smaller integrated intensities, and in order to obtain a measurable signal it is necessary to increase the incident intensity. In addition, for these crystals, the separation between reflection in reciprocal space becomes smaller so that a highly collimated beam is needed to achieve the required order to order resolution. These two requirements make SR an outstanding source in macromolecular crystallography.(see 3.1.1)

2.8 Polarization.

The high degree of polarisation of SR in the plane of the orbit (horizontal plane) (see the polarisation factor in Eq. 41) indicates that although there are technical problems, a vertical scattering plane which also uses the high intrinsic collimation of SR is more favourable. The polarisation factor for each reflection should be carefully calculated, even if this is in general more difficult than in the case of non-polarised characteristic radiation from conventional sources.

2.9 Absorption and fluorescence

In the monochromatic beam method, absorption can be diminished by using a short wavelength or one for which the absorption of the sample is minimal. Here again, the advantage of having the possibility to select any wavelength from a continuous spectrum is obvious. In a similar way one can reduce the fluorescence radiation from the

sample, which often obscures the measurements.

2.10. Extinction

As is well known, extinction decreases with decreasing wavelength and thus extrapolation to zero wavelength of the signal measured at different wavelength enables - at least in principle - to obtain extinction-free data. In any case, the tunability of SR permits a direct test of the occurence of extinction and its reduction by the use of an incident monochromatic beam with a shorter wavelength. In the white beam method the wavelength dependent extinction causes some difficulties.

3. . Applications of Synchrotron Radiation

3.1 Crystal structure determination

3.1.1 Introduction

Perhaps not unexpectedly there have been, until now, relatively few experiments using SR in this field except for biological applications. The reasons for this situation are to be found in the differences, both qualitative and quantitative, between macromolecular and conventional crystallography as explained below.

As shown previously, the integrated intensity of a Bragg reflection in the case of monochromatic incident radiation is proportional to

$$i_o \; \lambda^3 \; A \; \frac{V}{v_o^2} \qquad (47)$$

where i_o is the incident intensity on a crystal of volume V, unit cell volume v_o and absorption factor

A for the wavelength λ.

The inverse relationship between the integrated intensity and v_o implies that as v_o increases the total elastic scattering by electrons in the sample is distributed over an increasing number of reflections which are on average weaker. Another complication arises from the fact that proteins in the crystalline state are less ordered than is usually the case for small molecules. This disorder is static as well as dynamic so that the diffraction pattern usually does not extend to the limit set by the wavelength. Further, it it difficult to obtain large protein crystals. Crystals with dimensions of 1 - 2 mm corresponding to the optimal thickness given by the inversion of the linear absorption coefficient for wavelength around 1.5 Å can only rarely be obtained. Finally, protein crystals are also very sensitive to radiation damage, the higher order reflections which contain information about the details of the structure being more affected. It appears that radiation damage is to a large extent due to the formation of free radicals and, once started, degradation continues regardless whether the crystal is still exposed to X-rays or not. The most obvious solution to all these problems is to

increase the intensity of the incident radiation and this is what, among other reasons, made SR attractive to protein crystallographers (for a review see Bartunik et al., 1982).

3.1.2. Macromolecular crystallography.

3.1.2.1. Experimental

For macromolecular crystallography one has to consider, besides intensity, another important parameter which is the signal to noise ratio at the detector. In the case of film, the S/N ratio is enhanced when the spot size is small because this detector responds to the number of quanta per unit area. Electronic detectors are not subject to the same limitation, but again a small spot size is desirable to obtain a good separation of adjacent spots (order to order resolution).

The bandpass of the monochromator must be narrow enough to have a negligible effect on the spot

size. For a continuous source, only perfect crystals are adequate in this respect. Full use of the available photons for these applications can thus only be achieved using narrow bandpass demagnifying, focusing optics. Until now most normal and high resolution data collection in macromolecular crystallography, has been performed using film. (For a general discussion see Fourme (1979)). Monochromatisation and focusing in the horizontal plane are obtained by assymmetrically cut curved crystal monochromators. An adjustable cylindrical curvature can be conveniently achieved with a triangular shaped Ge(111) crystal mounted in a cantilever fashion. (Lemonnier et al. (1978), Hendrix et al. (1979)). The optimal settings for such systems have been calculated by Helliwell and Worgan (1981). A log-spiral curvature monochromator has been described by Webb et al (1977). The main drawbacks of these devices are the wavelength dependence of the bandpass (Lemonnier et al. (1978)) and the rotation of the monochromatic beam in the horizontal plane when the wavelength is changed.

Focusing in the vertical plane is obtained by total external reflection of the X-ray beam by mirrors, which also removes most of the higher

order harmonics.   Satisfactory results have been obtained with segmented mirrors (Hendrix et al. (1979)).   Usually, with existing sources, the cross-section obtained with mirror - monochromator devices is approximately 0.5 x 0.5 mm^2 so that most of the beam is intercepted by crystals with normal dimensions. The slight convergence of the beam is optimal as far as angular resolution and film detection are concerned, as illustrated in figure 11.

The focused monochromatic beams can be best compared with that of a rotating anode source with mirror - monochromator focusing. The convergence angles are similar and provide the high angular resolution which is required to study crystals with large cell dimensions, but the beams obtained from SR sources are approximately two order of magnitude more intense with the additional advantage of tunability.

The comparison with non-focused, collimated divergent beam from rotating anodes is less straight-forward: The gain in intensity is smaller but the quality of data is much higher with SR due to the focusing geometry.

Precession cameras were used for data collection in the early feasibility studies (Phillips et al.

1976), whereas nowadays full three-dimensional data are routinely collected with modified Arndt-Wonacott oscillation cameras. (Lemonnier et al.   1978;   Fourme 1979, Bartunik et al., 1981). Scaling errors due to intensity fluctuations of the source can be compensated by monitoring the incident beam intensity with a small ionization chamber placed between the collimator and the crystal (Bartunik et al. 1981). Processing and digitizing of films which are recorded at rates of 100 - 700 per 24 hours is a considerable problem. Data reduction is done in the conventional way, except for a modified polarisation correction (Bartels, 1981).

Data have also been collected with a modified four-circle diffractometer (Phillips et al. 1979) on a focused monochromatic beam obtained from a toroidal mirror - double crystal system (Hastings et al. 1978). This instrument is accurate but its data collection efficiency for complex structures is too low when equipped with a single detector.   For this reason there is considerable interest in the development of area detectors which hopefully will supersede film for many crystallographic applications in the near future, although one should be aware that many problems

still remain to be solved. The most popular systems are based on multiwire proportional chambers (MWPC) which are photon counting detectors. Several systems oriented towards macromolecular crystallography with SR are in various stages of development at Stanford (Phizackerley et al. 1980), Novosibirsk (Baru et al. 1978), Hamburg (EMBL) (Gabriel et al. 1978) and Orsay (Charpak et al. (1978), Kahn et al. (1980)). Another approach is based on an integrating TV detector (Arndt and Gilmore 1979).

3.1.2.2. Results.

The feasibility studies were made with various crystals, including small crystals and crystals with a very large unit cell using relatively low X-ray fluxes (Phillips et al 1976; Harmsen et al. 1976). Full three-dimensional data have since been collected at higher intensities for perhaps twenty five native protein crystals and heavy atom derivatives, using dedicated oscillation cameras installed at DCI and DORIS (Fourme 1979 and Bartunik et al., 1981). A large part of this

data has been fully processed, general features have emerged:

The angular resolution and signal-to-noise ratio of pictures compete in quality with those obtained with the best conventional equipment, i.e. rotating anode X-ray tubes with mirror - monochromator optics.

A higher dose rate is favourable for data collection and more data will be, in most cases, collected from a given crystal with SR. As a result, data are usually obtained at higher resolution and smaller crystals can be used. Useful data has been collected for crystals with dimensions as small as 50 - 100 μm. Further reduction of the crystal size would, however, require a substantial reduction in parasitic scattering as well as new methods of sample handling. First experiments also indicate that even better results can be obtained with low temperature equipment due to a reduction of radiation damage and thermal motion. A low temperature device for use with SR has been described by Bartunik and Schubert (1981).

A number of groups are in the process of building electron density maps or refining their models, using SR data.

3.1.3 Anomalous scattering.

3.1.3.1 Introduction

The feature of SR which is perhaps most attractive to crystallographers and especially protein crystallographers is the tunability of the source. Already now, wavelength shorter than that of the traditional CuK_α line are increasingly used to obtain higher resolution data or to decrease the magnitude of the absorption correction.

However, the main asset of tunability results from the possibilities given by the use of anomalous scattering techniques, which can be applied most efficiently when the structural unit contains one or several atoms with absorption edges in the range of $0.6 - 3.1 \text{Å}$, i.e. elements with $Z \geqslant 51$ (L edges) or $42 \leqslant Z \leqslant 20$ (K edges). The traditional solution to the phase problem in macromolecular crystallography is Multiple Isomorphous Replacement (MIR) (Green et al. 1954). The method relies on changes in scattering produced by isomorphous metal substitutions and requires the native crystals plus at least two

isomorphous derivatives. Suitable derivatives are often difficult to obtain and isomorphism is always, to some extent, imperfect.

Another source of phase information is derived from anomalous scattering by the heavy atom(s) bound to the macromolecules (see 1.4). The real part f' of the anomalous scattering has a phase equal to that of the normal scattering and the imaginary part f'' is phase-advanced by $\pi/2$; thus in noncentrosymmetric crystals, Friedel's Law ($F(\vec{s}) = F(-\vec{s})$) is no longer obeyed. Measurement of Bijvoet pairs ($F(\vec{s})$ and $F(-\vec{s})$) can resolve the phase ambiguity so that only the native crystal and a single heavy atom derivative are required as illustrated in figure 12. (Single Isomorphous Replacement plus Anomalous Scattering or SIRAS). Although a few structures have been solved by this method, it is more frequently used to improve the accuracy of phase information derived from multiple isomorphous replacement (Blow 1958). Anomalous scattering effects alone can be used to completely determine the phases (Raman 1959), as the real and imaginary parts of the anomalous scattering are wavelength-dependent. Changes in the real part are analogous to isomorphous replacement. Thus measurements using several

different wavelengths and a single derivative are in principle sufficient to solve the phase problem. If Bijvoet pairs are measured, two wavelengths are required as shown in Figure 13; if the Bijvoet pairs are not measured, each reflection must be measured at three wavelengths. The largest changes in the f' and f'' values are observed when the wavelength is varied close through an absorption edge of the anomalous scatterer.

Whereas conventional sources with their characteristic emission lines strongly limit the scope of multiple wavelength experiments (Hoppe and Jakubowski, 1975), the easily tunable narrow bandpass X-ray beam available at SR sources offers tremendous possibilities for these measurements.

Although only few multiple wavelength experiments have yet been reported with SR, many efforts in the development of methods and data acquisition are converging to allow routine use of these techniques at least for macromolecules of medium complexity.

3.1.3.2 Methodology

To start with, the anomalous scattering terms must be determined as a function of λ . f'' is related to the absorption cross-section $\sigma(\omega)$ and can be found by least squares refinement from diffraction experiments (Phillips et al. 1978) or from absorption experiments using an EXAFS instrument (Templeton et al. 1980a). f' can be also derived in diffraction experiments, from absolute intensity measurements (Freund 1975) or from interferometry (Bonse and Materlik 1976). f' and f'' are related by Kramers Kronig relationship (see section 1.4). Sharp anomalies in the absorption spectrum on the high energy side of an absorption edge – the so-called white lines – are frequently observed in EXAFS spectra. The corresponding amplitude modulations of f'' and of f' are of special interest because both components are substantially modified over a narrow range of wavelengths. This is the case for e.g. Caesium (L-edges) and cobalt (K-edge) (Phillips et al. 1978).

There are several ways to use anomalous scattering:

- optimised f''-SIRAS method

The method of SIRAS is useful where only a single isomorphous derivative can be obtained and is especially suitable for a large protein with little or no centric data. λ should be chosen so as to maximize f''.

The measurement of Bijvoet pairs may be avoided if data are collected at two wavelengths on both sides of an absorption edge (Arndt 1978).

- two (three) wavelength method with (without) Bijvoet pair measurements.

To use this approach f' must be substantially different for the various wavelengths. The method is well suited for studies of metalloproteins or proteins for which only a non-isomorphous derivative can be prepared.

Measurements at three different wavelengths, without Bijvoet pair information are analogous to the measurement of the native form and two derivates because of the variation of f' with (Herzenberg and Lau 1967).

Measurements of Bijvoet pairs at two wavelengths on both sides of an absorption edge give also a unique value for the phase.

Various data collection strategies for

multiwavelength measurements have been analysed by Phillips and Hodgson (1980), using computer simulations with the anomalous scattering data from cesium. They estimated the lower li; le mean phase error for various schemes, ... ing errors in intensity measurements and protein molecular weight. The results show that the usefulness of these methods is clearly related to the development of fast and accurate data collection methods.

Multiwavelength experiments on protein crystals with SR have been reported by Phillips et al. (1977), Phillips (1978) and Bartunik et al. (1979).

The experimental requirements of multiwavelength methods have been discussed by Arndt (1978) and Fourme (1979). The instruments have to be equipped with a narrow bandpass monochromator, allowing fast and accurate tuning as well as an electronic area detector designed for accurate intensity measurements at high count rates. Multiwire proportional chamber or TV- systems will probably fulfill these requirements.

3.1.3.3 Application to small and medium-sized structures

Anomalous techniques will certainly be extremely useful for the determination of medium-sized structures, an area where heavy atom methods and direct methods are still difficult to use and where isomorphous derivatives are rarely obtained. Many interesting substances fall in this category. An example is provided by a polypeptide, cation bound gramicidin A for which anomalous data were collected at a wavelength where the f''-value of the anomalous scatterer (cesium) is maximum, resulting in an improved electron density map. (Phillips, 1978).

3.1.4 Crystallography of samples in special environments

In all experiments of this type both the incident and scattered beam must penetrate some windows and thus the recorded intensity is reduced by absorption. In some cases (e.g. samples in a

diamond anvil cell) the sample is very small (of the order of 10^{-3} mm^3) and there are some restrictions concerning the available range of the scattering angle. Thus the tunability, the high spectral brightness and high intensity, and the possibility - whenever appropriate - to use the energy-dispersive method makes SR sources ideal for this type of studies. So far only a few high pressure experiments - some as feasibility studies - have been performed (Buras et al. 1977, Buras et al. 1978, Benedict et al. 1980, Hinze et al. 1980, and Olsen et al. 1981 at DORIS; Skelton, 1980, Manghnani et al. 1981 and Ruoff, 1981 at SSRL). All these studies were done on powders and have clearly demonstrated the great advantage of energy dispersive diffraction at SR sources for high pressure work. For example, at DORIS (electron energy 4-4.5 GeV, 20 - 40 mA) useful diffraction patterns were obtained in 500 - 1000 sec. (at least one order of magnitude faster than at conventional sources), with improved resolution and a better peak-to-background ratio. Figure 14 shows, as an example, the diffraction pattern of powdered YbH_2 at atmospheric pressure and at 282 kbar in a diamond anvil cell (Olsen et al. 1981). Owing to the very good collimation of the incident

SR beam the diffraction lines originating from the gasket, which usually obscure the pattern, are absent.

As concerns high temperature studies again only a few test-experiments have been performed. A follow-up of the Mn-αMn-β phase transformation and thermal expansion coefficient measurements of Mn-α in the range of 25°C - 690°C (Buras et al. 1977) and the study of Y_2O_3 in the temperature range of 25°C - 1900°C (Buras et al. 1980b) using the energy-dispersive technique at DORIS were reported. Recently, Manghnani et al.(1981) have performed energy dispersive X-ray diffraction measurements at SSRL on MnF_2 and FeF_2, simultaneously at high pressures and high temperatures (250°C), using a diamond anvil cell.

3.1.5 Differential crystallography.

3.1.5.1 Introduction.

The variation of an external parameter e.g. temperature, pressure, stress, magnetic or

electric field ,applied to a single crystal can induce structural modifications which are reflected by small variations of the intensities and/or positions of the Bragg peaks. A quantitative description of these modifications can be derived from very accurate intensity measurements, using differential techniques to minimize experimental errors, and the variations of the relevant structural parameters can be obtained from the differential intensity data by least squares methods. These procedures are also applicable to the study of weak effects like magnetic scattering. The data can be collected using a diffractometer with a single counter measuring predetermined reflections for short periods in a cyclic manner and integrating the signal corresponding to the same values of the variable parameter separately. This procedure has to be repeated for a sufficient number of reflections, depending on the problem. With SR the times required to achieve suitable counting statistics are considerably shortened. This also reduces the experimental constraints e.g. mechanical stability, extreme temperature or pressure conditions etc) and makes the study of very weak effects a practical proposal.

Two applications of these methods will be discussed here. The first uses the unusual polarization characteristics of SR and the second relies on the tunability of the source.

3.1.5.2. Magnetic diffraction.

Diffraction of X-rays is usually interpreted in terms of the Thomson scattering mechanism (see 1.2). It would thus seem that X-rays only give information about charge density, the electron spin density being ignored. In fact, as already pointed out, the magnetic moment associated with the spin also interacts with the magnetic field of the incoming radiation, th spin dependent part of the scattering amplitude being roughly proportional to the momentum transferred from the photon to the electron. In elastic scattering the transferred momentum, i.e. the scattering vector, is of the order of $\hbar/r$ (r :Bohr radius). As a result, spin effects can usually be neglected. The magnitude of the effects to be expected in X-ray diffraction from magnetic compounds was first calculated by Platzman and Tzoar (1970) and

the predictions were confirmed by the experiments of de Bergevin and Brunel (1972). Further experiments made with a standard source on antiferromagnets and ferromagnets have been published together with the basic formulae (Brunel and de Bergevin, 1981, de Bergevin and Brunel, 1981).

In the case of antiferromagnetic structures ,e.g. hematite, the symmetries of the atomic magnetic moments result in superstructure reflections with intensities which are of the order of 10^6 times weaker than those of the structure reflections. For ferro or ferrimagnetic compounds, the order between magnetic spins does not affect the periodicity nor the space group, but the theory predicts a weak supplementary term to the Thomson scattering intensities as observed on iron and zinc spinels with standard sources. Experiments on zinc spinel have been complemented by measurements with circularly polarized X-rays emitted by a storage ring (Brunel et al. 1979). In this case, the additional term is given by T F $\underset{\sim}{S}.\underset{\sim}{Q}$, where T is the rate of circular polarization, F the Thomson scattering structure factor, $\underset{\sim}{S}$ is the magnetic structure factor (spin density) and $\underset{\sim}{Q}$ is a geometrical term. As illustrated in Figure

15 the instrument used at LURE-DCI consists of a vertical axis goniometer installed behind a curved crystal monochromator. The device can be translated vertically across the beam to change the degree of circular polarisation. The powdered sample was magnetized along the sum of the incident and diffracted wave vectors, and the magnetization was inverted every 20 seconds. The relative differences ($\Delta I/I$) between the two intensities derived from measurements for several reflections were in good agreement with the theoretical values.

Apart from this particular experiment, magnetic scattering may be complementary to neutron diffraction to determine spin arrangements because of the difference in interaction between X-ray photons and spins and between neutron and spins. Other possible applications concern the study of compounds which are highly absorbing for neutrons. Conversely, due to the weak penetration of X-rays in bulk matter, this radiation can be used to analyze magnetic effects near a surface or in thin materials.

3.1.5.3. Anomalous scattering studies

Experiments with Cr K_α radiation have shown that the application of an electric field to a rutile crystal induced small changes in the intensities of Bragg peaks. From the analysis of these variations as a function of the wavelength, it is possible to derive f' and f''-values for the titanium ion. Preliminary measurements have been performed across the titanium K-absorption edge. (Lissalde et al. 1979) using SR with a tunable monochromator.

3.1.5.4. Photochemical perturbation.

The photodissociation reaction of the complex between carbon monoxyde and the protein myoglobin (CO-Myoglobin) is being studied by Bartunik et al. (1981). In these experiments which aim at establishing changes in the tertiary structure of myoglobin, a Xe^* Cl excimer laser pumping a dye (Rhodanese 6G) laser, which delivers a 10 ns pulse of approximately 200 μJ at 590 nm with a frequency

of 5Hz, is used to irradiate a small crystal (200 X 200 X 30 μm^3) of CO-Myoglobin cooled to -20°C. The time course of the intensities of a selected set of Bragg reflections is followed with a time resolution of 500μs using a position sensitive detector. Several relections show a very significant change (increase or decrease) of intensity immediately after the laser flash followed by an exponential relaxation ($t_{1/2} \simeq 3$ ms). This can be interpreted as the rate of rebinding after production of a transient deoxy state by the laser flash. Thermal effects seem to be negligible under the experimental conditions and shifts or broadening of the reflections have not been observed.

3.1.6. Accurate measurement of structure factors. Electron density distribution and chemical bonding.

Charge density determinations are generally carried out by a combination of X-ray and neutron diffraction. The X-ray data yield the electron density whereas the neutron data give the

positions and thermal parameters of the nuclei. Until now, these studies have provided qualitative and, to a lesser extent, quantitative results which can be correlated with other physical measurements (e.g. Compton scattering) and with quantum chemical calculations. Accuracies of the order of 1% can be obtained for the structure factors and an improvement of a factor of 10 is aimed for.

Available results are limited by systematic errors due to extinction, absorption and multiple diffraction. Further, the lack of suitable sources and detectors limits the collection of the large number of high order reflexions which are accessible at low temperature. For complex systems, data collection times become impractical with conventional equipment.

SR sources have potentially several advantages for this type of studies. Their high intensity would allow to collect high order and quasi-forbidden reflexions which carry important electronic and vibrational information in comparatively short times. The reduction in data collection time would also substantially simplify the experiments since, for instance, the crystal would only have to be kept at low temperatures for a few hours or

days instead of weeks or months.

The high brilliance of the source would allow to reduce the size of the sample which in turn would reduce absorption and extinction as well as eliminate many of the uncertainties presently associated with structure factor measurements. Further reduction of absorption and extinction can be achieved by using short wavelengths which are readily available from high energy storage rings with critical wavelengths of 1 $\mathring{A}$ or below or from wiggler magnets. The short wavelengths also give the possibility to increase the resolution (see section 2.3). The plane polarized nature of SR provides a way to eliminate extinction effects from single crystal data using a method suggested by Mathieson (1977). This method involves the reflexion of plane polarized X-rays diffracted in the π -mode (Compton and Allison, 1935) from a crystal plane. Measurements of integrated intensity are made over a range of 2θ on either side of $2\theta = 90°$ and a suitably chosen function of the intensities is plotted against 2θ and extrapolated to the limit $2\theta = 90°$. The prerequisite for this method is a tunable source of plane polarized X-rays. Combination of a channel-cut monochromator and a solid state

detector would provide the basis for such measurements with SR. The beam has a steady decay in intensity (≈ 0.1 % per minute). Further, with present day sources, the positional stability and short term intensity fluctuations are limiting factors. The available area detectors do not yet have the required accuracy for most measurements. However, if the present rate of development continuous one may envisage the development of electron density determination into an analytical technique of general applicability.

3.1.7. High resolution powder studies.

High resolution powder diffraction patterns can be obtained using a triple axis spectrometer with SR (see Section 5.1.3.4). Preliminary data obtained at HASYLAB by Buras for naphtalene show a full width half maximum (FWHM) of $0.025°$ ($\lambda =$ 1.54 $\mathring{A}$, $2\theta =$ 19°) which corresponds to an improvement of a factor of 5 compared with patterns obtained with conventional sources. Higher resolution powder diffraction patterns in conjunction with the Rietveld (1969) profile fitting method should make

it possible to extend structural studies on powdered samples to materials with larger unit cells.

3.2. Topography

3.2.1. Introduction.

X-ray topography (XRT) is a non-destructive imaging technique providing a map of extended defects in quasi-single crystals. The method is based on the differences in reflecting power between perfect and distorted regions of a crystal which manifest themselves in the intensity distribution within a Bragg reflection. The nature and the dimension of the defects can be deduced from the intensity profile, the interpretion of the observations being mainly based on the dynamical theory of diffraction. Topographic techniques for SR are described in detail in a recent review (Sauvage and Petroff, 1980). They will only be discussed very briefly here and illustrated with some applications. Both

the white beam technique (WBT) and the monochromatic beam technique (MBT) will be described.

3.2.2 White beam topography (WBT)

3.2.2.1 Experimental techniques, advantages and limitations.

WBT is based on the Laue technique: Any crystalline material immersed in a white X-ray beam diffracts along given directions, according to Bragg's law:

$$2 d_{hkl} \sin \theta = \lambda \qquad (48)$$

provided the reflection HKL is not systematically absent. Each spot in the Laue pattern is a topograph (Guinier and Tennevin 1949, Schulz, 1954). High resolution experiments require geometrical resolutions of a few microns and an SR source with its very low divergence is an exceptional tool in this respect (Tuomi et al.

1974; Hart, 1975) as illustrated in Figure 16.
The maximum geometrical resolution (R) is given
by:

$$R \simeq S \, p' \, p \qquad (49)$$

for a source with average dimension S, a sample to
source distance p and a sample detector distance
p' provided $p \geqslant S f^{-1}$ where f^{-1} is the apex angle of
the cone in which each point of the source emits
X-rays. The latter requirement is achieved for
all X-ray storage rings for values of p larger
than 20 m. Since the value of p' is usually about
5 cm resolutions between 1 and 15 μm can be
achieved with existing sources (1mm$\leqslant$ S $\leqslant$ 6 mm) us
ing large values of p, of the order of 20 to 50 m.
The experimental setting is simple although great
care must be taken to obtain a satisfactory signal
to noise ratio. The main parts of the instrument
are a shutter or chopper, a slit system, a
remotely controlled goniometer and a detector:
film systems with automatic plate changer or high
resolution TV detector. Since sample-detector
distances of 10 or 20 cm can often be tolerated
bulky ancillary equipment e.g. magnets, furnaces,
cryostats can be installed around the sample
without too many problems. In addition to being
relatively simple to use, the WBT has several

advantages:
- Since the spectrum of the incident SR is
continuous there is no need for accurate
orientation of the crystal and the WBT is able to
accomodate any slight modification induced by the
changes in environment (e.g. stress, temperature,
electric field). Warped crystals and sample with
subgrains or grain boundaries can be properly
imaged. Reconstructed topographs of
polycrystalline samples have also been obtained
(Stephenson et al. 1978).
- Contrary to the conventional Lang method (1959)
two dimensional pictures can be obtained without
scanning.
- The various spots which are recorded
simultaneously provide complementary information
about the same sample and allow quick defect
identification.
These features added to the high intensity of SR
lead to an enormous reduction of the time scale of
the experiments without sacrifice of information.
Exposures with high resolution photographic plates
take only a few seconds or minutes. Although TV
cameras provide real time detection the resolution
and sensitive area of these devices must be
significantly improved to compete in quality with

film. (Sauvage, 1978)

The main limitation of the WBT lies in the difficulties involved in computing the contribution of the various harmonics to an image as well as in comparing the integrated intensities of different images. Little attention has yet been paid to the study of defect contrast in this method (Miltat, 1980). Further limitations arise from the fact that the WBT is not sensitive to warpage which makes separate imaging of misoriented areas which are superimposed in the beam path difficult.

3.2.2.2. Applications.

In most applications which have been r: ..ed so far, the effect of modifications of t.. ..ple environment on the crystal organisation was followed by rapid sequences of topographs. The relevant parameters, which are varied in kinetic experiments, are, for instance, mechanical stress, thermal treatments and magnetic or electric fields.

Results have been published on plastic deformation

(Miltat and Bowen, 1979), recrystallisation and crystal growth (Gastaldi and Jourdan, 1978, Mac Cormack and Tanner, 1978, Jourdan and Gastaldi, 1979, Gastaldi and Jourdan, 1979), misfit dislocations and phase transitions (Bordas et al. 1975, Petroff and Sauvage, 1978), polytypes (Steinberger et al. 1977), magnetic domains (Tanner et al. 1976, Sery et al. 1978, Safa and Tanner, 1978, Chikauba and Tanner 1979, Clark et al. 1979, Stephenson et al. 1979). Other papers are more technique oriented (Tanner et al. 1977, Buckley-Golder et al. 1977, Stephenson et al. 1978, Hartmann, 1977, Miltat and Dudley, 1980) or present a review of the field (Authier, 1977, Sauvage and Petroff, 1980, Miltat, 1980)

Further progress in kinetic experiments is dependent on the availability of better electronic detectors and especially of storage rings with higher spectral brilliance. Improvements in these areas would allow to lower the time resolution down to a few milliseconds which would be adequate to study, for instance, crack propagation or plastic deformation under high stress (Farge and Duke, 1979).

3.2.3. Monochromatic beam topography (MBT)

3.2.3.1. Experimental.

MBT (for a recent review see Sauvage, 1981) is complementary to WBT but requires more elaborate experimental arrangements like those developed for second generation experiments both at LURE-DCI (Orsay) (Sauvage, 1978), SSRL (Stanford) (Parrish and Erickson, 1978) and HASYLAB (Hamburg) (Bonse and Fisher,1981)These instruments are especially designed high accuracy two axis spectrometers which preserve polarization and take advantage of the smaller vertical divergence by having all diffracted beams confined in the vertical plane. The monochromator, mounted on the first axis, is tailored to meet the experimental requirements in terms of bandpass, exit divergence, tunability, harmonic rejection and tail suppression. Among other possibilities it can be designed to have a bandpass and a divergence similar to that of a conventional source with, however, the advantage of higher intensity and tunability. Usually, the monochromator is a grooved silicon or germanium

single crystal with one or more reflections (see Chapter 4) It should be mentionned that the most important parameter in the interpretation of images is the ratio of the divergence $\Delta\theta$ of the monochromatized beam and the intrinsic width (δ) of the sample reflection profile. When $\Delta\theta << \delta$ the plane wave contrast theory applies, whereas for $\Delta\theta >> \delta$ the kinematic theory dominates in low absorption wafers (Sauvage and Petroff 1980).

3.2.3.2 Applications.

The MBT was used to obtain stroboscopic observations of time dependent distortions of moving magnetic domain walls and wall junctions in Fe-Si single crystals as shown in figure 17 (Miltat and Kleman, 1979). Pseudo-plane wave topography can be performed with monochromators combining parallel and antiparallel reflections. These devices deliver a very parallel and highly monochromatic beam which closely approximates a planar X-ray wave (Kohra et al. 1978, Takagi et al. 1978) thus allowing very detailed studies of deformations in crystals (e.g. defects, growth

sectors, heterojunctions, magneto- and electrostrictive distortions). As the theory of contrast is relatively simple in this case a quantitative interpretation is also possible. The first SR plane wave topographs were recorded at LURE with a very parallel and monochromatic beam (divergence 0.3", spectral width $\sim 7 \; 10^{-6}$) extracted from the white beam by a multiple reflection monochromator. Separate images of a quaternary epilayer($Ga_{0.7}Al_{0.3}As_{1-y}P_{y}$) and a GaAs substrate building up a nearly matched heterostructure were obtained (Petroff et al, 1980) and analysed using an image simulation programme (Riglet et al., 1980).

The method can be made highly strain sensisitive by rotating the crystal slightly out of the Bragg condition on the steepest part of the rocking curve or, alternatively, high spatial resolution can be obtained by adjusting the crystal on the remote wings of the rocking curve.

Second generation storage rings should provide even better monochromatization and parallelism of the wave while retaining reasonable intensity. Hence, the sensitivity of the method could, in principle, be increased to allow, for instance, to detect relative differences in parameters of the

order of 10^{-4} to 10^{-5} in a multiple heterostructure (Farge and Duke, 1979).

3.2.4. Summary.

-Both the WBT and the HBT are usable with SR as opposed to conventional sources where the WBT is impractical because of the low spectral brilliance of the Bremsstrahlung.

- As a result of the low divergence of SR and the small source size, the local horizontal and vertical divergences of the incident beam at any point of the sample depend only on the horizontal and vertical angle subtended by the source at the sample location- usually between 10^{-3} and 10^{-4} radians. This is important both for the WBT where the geometrical resolution depends only on the local divergence and for the HBT which uses perfect crystal monochromators with a narrow acceptance.

-The continuous spectrum of SR covers the basic requirements for the WBT whereas any wavelength can be selected for the HBT.

-The high flux is essential for shorter exposures,

real time imaging and dynamic experiments.

- The lateral and, to a lesser extent, the vertical extension of the SR beam allow imaging of relatively large samples.

- The pulsed nature of SR sources can be exploited for stroboscopic experiments in the MHz range (Graeff et al. 1981).

- One of the difficulties in using SR results from the unusual polarisation properties of the beam which must be taken into account both in the design and in the interpretation of topographs, e.g. planar defect contrast in the WBT (see Miltat 1981).

3.3. X-ray optical studies.

3.3.1. Tensorial properties of crystals.

Many crystals exhibit orientation dependent properties at optical frequencies as a result of the tensorial nature of their dielectric susceptibility e.g. birefringence and rotary power. The search for similar properties in the

X-ray region (Moliere 1939) gave negative (Hart 1978) or controversial results (Cohen and Kuriyama 1978). A clear-cut answer was not obtained due to a lack of intense X-ray sources. These effects, if they exist, are expected to be very weak except at wavelengths close to an absorption edge. The features of SR (intensity, tunability and high degree of linear polarization) have given new impetus to this field of research.

The first SR experiments simply demonstrated the interaction of polarized photons with single crystals. Due to interferences, the intensity which is Bragg reflected by a perfect crystal in the transmission geometry is an oscillating function of the sample thickness. With wedge-shaped crystals a fringe pattern (Pendellosung pattern) is thus observed. The intensity distribution in this pattern is dependent on the orientation of the plane polarized wave with respect to the scattering plane. When the wave is inclined at 45 to the scattering plane components respectively normal (σ-case) and parallel (π-case) to the scattering plane which have very slightly different periodicities, are excited, add coherently and produce a beat pattern. This type of pattern was

first observed by Skalicky and Halgrange (1972) using a laboratory source. Similar results were obtained in much shorter exposures using a white beam topography instrument (Sauvage et al. 1977, Karabekov et al. 1977). The main difficulty in the SR experiments arises from the fact that the radiation is still insufficiently polarized in the orbit plane for high accuracy measurements (90-95%). Using a polarizing crystal monochromator with five reflections Sauvage et al.(1979) were able to obtain a polarization ratio of 10^{-6} and tried, until now unsuccesfully, to measure the rotary power of $NaBrO_3$ close to the absorption edge of bromine. The lack of success, however, sets an upper limit to the magnitude of the phenomenon.

3.3.2. Many beam diffraction.

Most studies of X-ray dynamical diffraction have concentrated on the two-beam case i.e. when only two points of the reciprocal lattice are close to the Ewald sphere. Multiple-beam diffraction requires an intense and highly collimated X-ray

beam because it is accompanied by a severe limitation of the accepted divergence. SR would be a unique source for such applications. Furthermore, the study of many beam dispersion surfaces might contribute to solve the phase problem of X-ray scattering for some special geometries (Hart and Lang, 1961; Post, 1977). Simultaneous diffraction of several beams within the sample can lead to coherent interference effects which carry information about the relative phases involved.

3.3.3. Interferometry.

3.3.3.1. Principles and applications.

X-ray interferometry (XIN) (for a recent review see Bonse and Graeff, 1977) was introduced by Bonse and Hart (1965). In an X-ray interferometer, a standing wave field is produced by coherent beam splitting. Recombination is accomplished either by the use of Laue-case diffraction (in which the diffracted wave leaves

the crystal through the face opposite to the entrance surface), by Bragg-case diffraction (when the diffracted wave originates in the entrance surface of the crystal) or by a combination of these two cases. Interference oscillations are produced by a phase shifter placed in one of the beam paths; this may be a wedge-shaped object which is translated or a plate which can be rotated. Insertion of the object (phase object) under investigation in the other beam path produces an additional shift of this pattern. Measurement of this shift provides a very precise determination of the real part of the refractive index of the material; hence, the real part of the forward scattering factor (i.e. for $2\theta = 0$) $f_o(\lambda) = Z + f'_o(\lambda)$ may be determined with an accuracy better than 10^{-4}. The variation of the imaginary part $f''(\lambda)$, which is proportional to the linear absorbtion coefficient $\mu(\lambda)$, (see section 1.4) may be obtained from a transmission measurement using the same instrument. These data are extremely useful not only for crystal structure determination but also because they provide accurate scattering cross-sections for comparison with theoretical calculations. Although interferometric f' measurements were

first carried out on conventional sources these experiments take obvious advantage of the continuous, intense spectrum of SR sources. (Bonse and Materlik (1975), Bonse et al. (1980), Materlik (1981)) Another application of SR in XIN has been the construction and operation of a three-beam interferometer using Bragg-case multiple beam reflection(Graeff and Bonse,1977). This apparatus improves the spatial resolution in phase contrast microscopy when compared to Laue-case interferometers. A few other potential applications of XIN with SR have been discussed. (Farge and Duke, 1979).

3.3.3.2 Apparatus

The general layout of the XIN instrument used for f' and f" measurements at DORIS (Bonse et al. (1980)) is shown in figure 18. The triple Laue-case interferometer is a silicon single crystal in which beam splitting, recombination and superposition are done by means of three wafers, using the 220 reflection with the fundamental wavelength λ_o. A twofold Bragg reflection

monochromator cut in a silicon single crystal is placed in front of the interferometer and used to select or reject one or more harmonics. Both crystals form a double crystal diffractometer in the non-dispersive (+,-) setting which is rotated as a whole to vary the wavelength. During the measurement, the sample is moved in and out, while the fringe pattern is recorded and the phase shifter is rotated. The effect of the sample thickness is eliminated by recording fringes simultaneously at two wavelengths (λ_o and λ_o/m or λ_o/n and λ_o/m where m and are integers). The absorbtion coefficient $\mu(\lambda)$ is determined in two ways: one relies on the influence of absorbtion one the fringe contrast and the other one on the measurement of the transmission of X-rays through the sample scanning the diffractometer about the θ_1 axis as illustrated in figure 18. The instrument is remotely controlled and linked to a minicomputer. $f'(\lambda)$ and $\mu(\lambda)$ curves can be produced in a few hours of measuring time.

4. Scattering by randomly oriented systems.

4.1. Introduction.

The theory of scattering by randomly oriented systems and its formalism have evolved to a large extent, partly for historical reasons, separately from crystallography. For the sake of simplicity, one can start the discussion from the fundamental formula for scattering by randomly oriented systems consisting of spherical atoms which was first given by Debye (1915):

$$I(\kappa) = A(\kappa) \, g(\kappa) \, (\vec{E_i} \cdot \vec{E_j})_\kappa^2 \sum_{m=1}^{N_o} \sum_{n=1}^{N_o} f_m(\kappa) \, f_n(\kappa) \frac{\sin \kappa \cdot r_{mn}}{\kappa \cdot r_{mn}} \qquad (50)$$

where $A(\kappa)$ is the absorption factor, $G(\kappa)$ is a geometrical factor which has a value of 1 when a cylindrical symmetry is used for data collection and r_{mn} is the separation between the pairs of atoms m and n.

Note that here $I(\kappa)$ is a continuous function of κ as opposed to the situation in crystals where

the (continuous) transform of the electron density distribution in the unit cell is sampled at the reciprocal lattice point.

Only two cases will be discussed here: liquids and solutions of macromolecules.

4.2. Scattering by liquids.

For simplicity reasons we restrict the discussion to isotropic monoatomic liquids and assume that the atomic scattering factors have a spherical symmetry. To describe the position of the atoms which have correlated motions one introduces the pair correlation function $g(r)$ which gives the probability of finding an atom at a distance r from an atom placed at the origin ($r=0$). For larger values of r there is no correlation and $g(r)$ approaches 1. Up to values of r corresponding to about an atomic diameter $g(r)=0$ as a result of the finite atom size. The function $g(r)$ N/V where N is the number of atoms in the sample and V its volume, gives the number of atoms per unit volume at location r and is called the number density.

The measurement of the diffracted X-ray intensity leads to the determination of the so called radial distribution function $4\pi r^2 \rho(r)$ which gives the number of atoms in a spherical shell of radius r and unit thickness centred on an arbitrarily selected atom at the origin.

The scattered intensity is given by a mofified expression of Eq.(50) which takes into account the fact that all atoms are identical.

$$I(K) = A(K) |f(K)|^2 G(K) (\vec{\varepsilon_i} \cdot \vec{\varepsilon_f})_k^2 \sum_{n=1}^{N_o} \sum_{m=1}^{N_o} \frac{\sin K \cdot r_{mn}}{K \cdot r_{mn}} \quad (51)$$

After the necessary corrections (e.g. Compton correction) it is possible to extract $I(K)$ from the measured intensity.

First consider the quantity $T(K)$:

$$T(K) = N_o^{-1} |f(K)|^2 \sum_{n=1}^{N_o} \sum_{m=1}^{N_o} \frac{\sin K \cdot r_{mn}}{K \cdot r_{mn}} =$$

$$|f(K)|^2 + N_o^{-1} |f(K)|^2 \sum_m \sum_{m \neq n} \frac{\sin K \cdot r_{mn}}{K \cdot r_{mn}} \quad (52)$$

Assuming that the probability of finding an atom

is a continuous function of r and that the number
of pairs lying between r and r+dr is $N_0 \, 4\pi r^2 \rho(r)dr$,

Eq.(53) is obtained.

$$I(K) = \frac{T(K) - |f(K)|^2}{|f(K)|^2} =$$

$$\int_0^\infty 4\pi r^2 \, \rho(r) \, \frac{\sin K \cdot r}{K \cdot r} \, dr \qquad (53)$$

or

$$I(K) \cdot K = \int_0^\infty 4\pi r \, \rho(r) \, \sin K \cdot r \, dr \qquad (54)$$

This integral is not convergent but, as shown by
Warren and Gingrich ( ) one can add and
subtract the integral $\int_0^\infty 4\pi r^2 \rho_0 \sin K r \, dr$ which is
nearly equal to zero except for very small values
of K , to obtain an integral which converges:

$$I(K) \cdot K = \int_0^\infty 4\pi r \left(\rho(r) - \rho_0 \right) \sin K \cdot r \, dr \qquad (55)$$

After Fourier transformation this yields:

$$4\pi r \left(\rho(r) - \rho_0 \right) = \frac{2}{\pi} \int_0^\infty K \cdot I(K) \sin K \cdot r \, dr \qquad (56)$$

Obviously if one measures $I(K)$, knowing $A(K)$,
$f(K)$, $G(K)$ and $(\vec{e}_i \cdot \vec{e}_f)_K$ one is able to determine
$i(K)$ which by Fourier transformation will give
the quantity $4\pi r(\rho(r) - \rho_0)$. If in addition the
average density ρ_0 is known it is possible to
calculate the radial distribution function.
Figure 19 shows the measured intensity and the
corresponding radial distribution function of
mercury measured by means of X-ray energy
dispersive diffraction using a conventional source
(Prober and Schultz, 1975).
To our knowledge SR has not yet been applied to
study the structure of liquids.

4.3. Scattering from solutions.

Macromolecules in solution can be thought of as
being immersed in a homogeneous medium with
electron density ρ_0 . The scattering amplitude
from a solution can then be considered to be the
sum of the scattering of this homogeneous medium
and of fictitious particles with an electron
density equal to the difference between their
density in vacuo and that of the homogeneous

medium. The phenomenon of low angle scattering is thus related to the presence of inhomogeneities in the electron density of the sample.

In a typical solution scattering experiment, all particles are identical and, as most SR experiments fall in this category we shall restrict the theoretical discussion to this particular case.

The particles are described by their excess electron density sometimes also called the electron density contrast:

$$\Delta \rho(\vec{x}) = \rho(\vec{x}) - \rho_o \qquad (57)$$

An equivalent description is given by the distance probability function p(r) which is the spherically averaged autocorrelation function of $\Delta \rho (\vec{r})$:

$$p(r) = \langle \Delta \rho(\vec{x}) * \Delta \rho(-\vec{x}) \rangle \qquad (58)$$

r^2 p(r) is the probability of finding a point inside the particle at a distance between r and r+dr from any other point inside the particle. For a real particle, p(r) has two main regions:

a) a region of sharp fluctuations due to the neighbouring atom pairs (1 $\mathring{A}\leqslant$ r $\leqslant$5 $\mathring{A}$) and of damped oscillations corresponding to structural domains (e.g. α -helix in proteins) for which 5 $\mathring{A}$ $\leqslant$ r $\leqslant$10 $\mathring{A}$.

b) A smooth region corresponding to longer intramolecular vectors. Beyond a certain value of r, (D_{MAX}) p(r) vanishes and all the vectors correspond to the solvent.

Since the scattered intensity and p(r) are related by a Fourier transformation as indicated in Eq. 59 there are alo two regions in the scattering curve .

$$K \cdot I(K) = 4\pi \int_{o}^{\infty} r \, p(r) \sin K \cdot r \, dr \qquad (59)$$

a) A region at small angles containing mainly information about the long range organisation of the particle (e.g. its shape)

b) a large angle region where the internal structure of the particles dominates.

The region of interest for the present purpose is the small angle region. Assuming that the experiment are performed under condi.   here

the absorption factors for the incident and the scattered beam are the same and that multiple scattering is negligible, Eq.50 simplifies to:

$$I(\kappa) = \sum_{m=1}^{N_o} \sum_{n=1}^{N_o} f_m f_n \frac{\sin \kappa \cdot r_{mn}}{\kappa \cdot r_{mn}} \qquad (60)$$

Since the scattering angles are small the relationships $\sin 2\theta = 2\theta$ and $\cos 2\theta = 1$ are valid and the polarisation corrections are no longer required. In the narrow range of κ the angular dependence of the atomic scattering factors can also be neglected. It should be stressed that in a small angle scattering experiment one is really trying to measure the scattering corresponding to small scattering vectors. For a given value of κ the angles are only small for a certain range of wavelength.

Typically, for a wavelength of 1.5 $\mathring{A}$, the small angle region extends to values of smaller than $(60 \mathring{A})^{-1}$. If the pattern were spread out by using longer wavelengths -not an impossible thing to do with SR- the formulae would have to be modified to take the angular dependence of the polarisation and atomic scattering factors into account.

Eq. 57 can be rewritten under a slightly different form:

$$\Delta\rho(\vec{r}) = (\rho_p - \rho_o) f_c(\vec{r}) + f_s(\vec{r})$$
$$= \bar{\rho} f_c(\vec{r}) + f_s(\vec{r}) \qquad (61)$$

ρ_p is the average electron density of the particle and ρ_o the average electron density of the homogeneous surrounding medium, e.g. solvent, $\bar{\rho}$, the difference between these two quantities is called the contrast.

$f_c(\vec{r})$ is a __dimensionless__ function which is independent of the contrast and in fact describes the effective volume of the particle. $f_s(\vec{r})$ is a function which describes the fluctuations of electron density inside the particle above and below the average value ρ_p .

By Fourier transforming Eq. 61 and multiplying by the complex conjugate one finds that the scattered intensity is:

$$I(\kappa) = \bar{\rho}^2 I_c(\kappa) + I_{cs}(\kappa) + I_s(\kappa) \qquad (62)$$

The three functions I_c , I_{cs} and I_s are the basic scattering functions or the characteristic functions corresponding to the shape (I_c), the

internal structure (I_s) and the convolution of these two (I_{cs}) (Stuhrmann and Kirste, 1967).

In a monodisperse solution, for instance, $\rho(\vec{\imath})$ will be identical for all particles and one will observe the square of the Fourier transform of the particles averaged over all orientations.

The simplest interpretation of the scattering curves relies on the Guinier approximation (Guinier and Fournet, 1955). At very low angles, the scattering curve can be described by the following equation:

$$I(\kappa) = I(o) \, exp \left(-\frac{R^2 \kappa^2}{3} \right) \qquad (63)$$

$I(0)$ is the extrapolated zero angle intensity and R is the radius of gyration of the particle.

For particles which have nearly homogeneous scattering density, i.e. in which $\rho_s(\vec{\imath})$ can be neglected, interpretation usually proceeds using simple models in a best fit calculation.

Eq. 62 suggests that in the case of particles which present large fluctuations in their electron density one can separate the basic scattering functions by changing the contrast and measuring different scattering patterns. This is the basis of the contrast variation method.

Generally, contrast variation is achieved by adding an electron dense solute to the solution, e.g. sucrose or a salt.

The technique relies, however, on the invariant volume hypothesis i.e. the volume accessible to the solvent must be independent of the contrast. The most straightforward way to obtain structural information for this kind of system is to make a plot of the square of the radius of gyration against the inverse of the contrast. Such a plot is fully described by the following equation (Ibel and Stuhrmann, (1975), Cotton and Benoit (1975))

$$R^2 = R_c^2 + \frac{\alpha}{\bar{\rho}} - \frac{\beta}{\bar{\rho}^2} \qquad (64)$$

where R is the radius of gyration at infinite contrast i.e. the radius of gyration of the shape.

α is the second moment of the internal structure ($\rho_s(\vec{\imath})$). The sign of α gives an immediate qualitative indication of the relative location of the regions of high and low scattering density. A negative value of α for instance means that the density increases towards the centre of the particle. The opposite situation will give a positive α whereas for homogeneous particles α is

zero.

The coefficient β is much harder to measure because accurate measurements at low contrast are required. It describes the dependence of the position of the centre of the particle on the contrast. In the extreme case of a two phase system i.e. a particle consisting of two homogeneous components with different scattering densities the relationship between β and the distance between the centres of the two phases (Δ) is given by (Koch et al. 1978) :

$$\Delta = \sqrt{\frac{\beta}{\rho_1^2}} + \sqrt{\frac{\beta}{\rho_2^2}} \qquad (65)$$

where ρ_1 and ρ_2 stand for the contrast at which the two components are matched.

It is clear that the structural information which can be obtained from a low angle scattering pattern is much smaller than with the data obtained from systems with three-dimensional order. Using a novel approach to the problem of the information content of a scattering pattern it was shown that the maximum number of independent parameters which can at most be extracted from a scattering pattern of a particle with finite dimensions is given by (Luzzati and Tardieu 1980):

$$J = \frac{K_{max}}{2\pi} \cdot D_{max} + 2 \qquad (66)$$

where D_{max} is the maximum distance between any two points in the particle and K_{max} the largest value of K for which data have been recorded. In the case of contrast variation experiments where one can separate the three basic scattering functions the number of independent parameters is 3J. Thus for a simple protein of molecular weight of around 10000 daltons, for instance, one can at best obtain five parameters. In practice, noisy data and systematic errors prevent one from achieving even this figure.

Given accurate data which extend far enough in reciprocal space, one can however obtain a substantial number of parameters for high molecular weight compounds. It is then up to the experimentalist to choose a base for the description of the structure. A promising and general approach is provided by the use of spherical harmonics (Stuhrmann, 1970).

SR presents great advantages for small angle scattering experiments. The high intensity, well-collimated beam provided by the source guarantees that a large amount of high quality data can be collected in a reasonably short time. It is thus not astonishing that most of the activity in the field has been oriented towards the solution of biological problems where the stability of the sample is a limiting factor. Further, biological macromolecules often consist of components with different electron densities, e.g. protein and nucleic acids in viruses so that contrast variation techniques can be used very profitably. Therefore, we have separated the biological applications from other studies although it should be realized that the same theories apply in all cases and that the same instruments are used.

4.4 Experimental techniques.

The various types of instruments for small angle scattering with SR have been described in a recent review (Koch et al. 1981). The systems used for

kinetic measurements are focusing (Lemonnier et al. 1978) and double focusing systems (Hendrix et al., 1979, Bordas et al., 1980). For anomalous scattering a non focusing, double monochromator system is required. (Stuhrmann and Gabriel 1981)

4.5. Applications of small angle scattering.

4.5.1. Biological applications of small angle scattering.

The main areas which have been investigated until now are:

a) Dilute solutions of weak scatterers

b) conformational equilibria

c) contrast variation

d) anomalous scattering

e) kinetic measurements

f) ultra small angle scattering

Examples of each of these types of experiments are discussed below. We have not attempted to make the traditional comparisons between SR and classical sources. Suffice it to say that most of

these experiments would not even have been attempted if SR had not been available. The latter combined with the development of high resolution, fast position sensitive detectors (PSD) is quickly modifying the traditional situation where data collection was the limiting step.

In fact, in all laboratories involved in SR the large quantities of data are already calling for new numerical techniques to handle them.

4.5.1.1. Dilute solutions and weak scatterers.

Good examples of this type of experiment are provided by the work done at DCI (LURE Orsay) on ribosomal proteins (Koch et al. 1981). The least one can say about the shape of these proteins is that it is a very controversial issue. Immuno electron microscopy and triangulation measurements seem to indicate that they have an elongated shape whereas neutron low angle scattering suggests that they are globular. The origin of these discrepancies (preparative methods, concentration, buffers) is not clear. In any case it is well known that the proteins show a strong tendency to aggregate so that one has to work at very low concentrations, typically between 1 and 4 mg/ml. High quality data have been recorded in one hour on the D11 camera at LURE for these small proteins (MW = 10000).

Another case where the drastic reduction of measurement time provided by SR makes all the difference is the study of Ca-ATPase of sarcoplasmic reticulum (le Maire et al. 1981). The evolution in time of a sample of freshly prepared active enzyme was studied. It showed

progressive aggregation of the particle and a concomitant reduction of activity. After a few hours, activity is completely lost. This phenomenon would make scattering experiments with a normal source impossible.

Other examples include the work of Hartt and Hendelson (1979) on muscle proteins done at SPEAR, of Dessen et al. (1979) on tRHA synthetases. There are several ongoing projects which fall in this category both at DCI (Orsay) and at the EHBL Outstation at DORIS.

4.5.1.2. Conformational equilibria

Host techniques used to study the mechanism of allosteric transition are spectroscopic and as opposed to small angle scattering not specifically sensitive to changes in the quaternary structure of the enzyme. The existence of possible intermediates between the two extreme states (T and R) can be detected by measuring the scattering pattern of the enzyme in the presence of variable concentrations of substrate or inhibitor. Further, the intensity of the beam is large enough

to contemplate kinetic measurements on these systems. Two examples have already been studied . In the case of ATC-ase (Aspartate transcarbamylase (E.C. 2.1.3.2)) a five percent change in the value of the radius of gyration was found when the enzyme was saturated with its inhibitor (PALA: N-(phosphonacetyl)-L-aspartate) (Moody et al.1979).

Preliminary evaluation of data collected on PFK (phosphofructokinase) indicates noticeable, although small, changes in the scattering pattern in the presence of adenosine triphosphate (ATP) and/or glucose-6-phosphate (Koch et al. 1980). Recently a study of the pH dependence of the structure of Tomato bushy stunt virus (TBSV) has been started at LURE (Kruse et al. 1981).

4.5.1.3. Contrast variation.

As already mentionned in section 4.3 the basic scattering functions can be separated using contrast variation if the particles have components which differ significantly in their electron density. A contrast variation study of

the 50S bacterial ribosomes which contain proteins ρ_e = 0.419 e/Å^3) and RNA (ρ_e = 0.472 e/Å^3) was started by Vachette (1980). Very accurate scattering curves were measured at several contrasts using sucrose as a contrasting agent. SR is a real breakthrough for contrast variation methods especially because exposure times on laboratory sources are most often prohibitive to contemplate this kind of experiment. SR focusing cameras cut the exposure times down to a few minutes per sample - a gain of 2 orders of magnitude even compared to rotating anode sources. This insures that complete studies can be carried out on a single preparation.

4.5.1.4. Anomalous scattering.

If the solute or the solvent contain an anomalous scatterer, Eq.(61) and (62) can be modified to take this effect into account (Stuhrmann 1980) yielding the following expression for the scattered intensity:

$$I(\kappa) = \left(\rho'^2 + \rho''^2\right) I_a(\kappa) + \rho'\left[\bar{\rho} I_{ac}(\kappa) + I_{as}(\kappa)\right]$$

$$+ \left[\bar{\rho}^2 I_c(\kappa) + \bar{\rho} I_{cs}(\kappa) + I_s(\kappa)\right] \qquad (67)$$

where ρ' and ρ'' are the real and imaginary dispersion corrections to the contrast. $I_a(\kappa)$ is the scattering function of the anomalous scatterers whereas $I_{ac}(\kappa)$ and $I_{as}(\kappa)$ are cross terms resulting from the convolution of the distribution of anomalous scatterers with the shape and the internal structure defined in Eq.(61)

Experiments have been performed by Stuhrmann (1980) using a solution of ferritin. This macromolecule consists of a core containing approximately 3000 iron atoms surrounded by a shell of twenty four protein subunits. A plot of the radius of gyration against the wavelength displays a sharp maximum corresponding to the absorbtion edge of iron as illustrated in figure 20. Obviously, by choosing appropriate salts for contrast variation one can use a solvent containing anomalous scatterers . Although in this case the extension of the traditional formulation using a complex contrast is trivial, this technique is probably the more general one from the experimental point of view. This approach has been used for protein solutions (Stuhrmann and Gabriel, 1981).

It seems likely that the extension of this method

,which has until now only been applied to biological samples, to the study of alloys or polyelectrolytes could be very fruitful. Another example of the potential of these methods is provided by the determination of the configuration of the iron atoms in hemoglobin (Stuhrmann and Notbohm, 1981). Although the real and imaginary contributions only amount to 0.1% and 0.001 % of the total scattering the results indicate that these effects can be measured with an precision of 10%.

The principles underlying these various experiments can be found in two recent reviews (Stuhrmann, 1981a, Stuhrmann, 1981b). Further, Stuhrmann (1981c) has described the advantage of extending these techniques to longer wavelengths, especially for biological material where the sulphur and phosphorus edges would become accessible.

4.5.1.5. Kinetic studies.

Two categories of phenomena are amenable to kinetic studies:

- Interactions between macromolecules e.g. assembly processes in biological systems.

- Conformational transitions.

The two cases which have been studied in detail so far fall in the first category where large differences in the signal can be expected.

Mandelkow et al. (1980) have investigated the polymerization of tubulin using a slow temperature jump. At $4°C$ this protein exists in the form of ring-like aggregates with a diameter of 350-400 Å whereas at $37°$ C in the presence of guanosine triphosphate (GTP) it forms long,hollow cylinders with a diameter of 220-260 Å called microtubules.The changes in the scattering pattern during polymerization induced by a sudden increase in temperature from $4°C$ to $37°C$ as well as during depolymerization resulting from the reverse transition are illustrated in figure 21. It is quite clear that immediately after the increase of temperature an intermediate state is formed in which rings can no longer be detected. This is

followed by the appearance of the characteristic scattering pattern of microtubules. Depolymerization seems to proceed directly from microtubules to rings suggesting that the two phenomea -association and dissociation- follow distinct pathways. With such relatively slow phenomena sufficiently accurate scattering patterns can be recorded in a single experiment with successive time frames of about 15 sec.

The second example is the dissociation of aspartate transcarbamylase which has been investigated by Moody et al. (1980) using stopped flow techniques. Under the influence of mercurials (e.g. p-chloro mercuribenzene sulphonic acid) the enzyme dissociates into two active catalytic trimers and three regulatory dimers. The reaction is interesting because of the connection between allosteric activation and dissociation in multisubunit enzymes. Using a circular detector with delay line readout built by A. Gabriel (1977) the dissociation process could be followed with a time resolution of the order of 100 msec, the required accuracy being achieved by accumulating the results of several experiments.

Figure 22 illustrates the changes in the scattering pattern of the solution during the reaction. The decrease of intensity in the low angle region corresponds to the dissociation of the large enzyme molecules and is compensated by an increase in intensity at larger angles resulting from the formation of free subunits. These first experiments have shown that studies of reactions in solution are feasible in practice with time resolutions in the range 10-100 msec. The main problem now lies in the development of high performance ancillary devices for X-ray work. Preliminary measurements on thermal phase transitions between $7^\circ C$ and $41^\circ C$ in the lipids of human low density lipoproteins were made at LURE with a time resolution of 100 msec (Aggerbeck et al. 1981). Similar experiments have been performed on bacterial lipids (Letellier et al., 1981).

4.5.1.6. Ultra Small angle scattering.

Some biological structures display periodicities of the order of microns. X-ray scattering from these structures cannot be resolved from the direct beam with conventional optics. Recently,

an instrument based on the design of the Bonse-Hart camera (Bonse and Hart, 1966) and making use of the excellent collimation and high intensity of SR was installed at the EMBL Outstation at DORIS (Bordas et al., 1982).

In this device, the sample stage is placed between a four reflection grooved crystal (Si 220) which also provides harmonic rejection and another four reflexion groove which acts as an analyzer.

Figure 23 shows a meridional diffraction pattern of frog Sartorius muscle obtained with this instrument, where the second order of the sarcomere length corresponding to a spacing of 26000 Å is clearly resolved. Few results are available yet, but the possibility to overlap with optical and electron microscopy is certainly very attractive for many problems in structural biology.

It should be noted that this type of instrument, which can be viewed as a very high quality triple axis spectrometer, is not restricted to low angle measurements. (See Sections 5.1.3.3. and 5.1.3.4. for possible applications).

4.5.1.7. Conclusions.

The small angle scattering experiments described above were done with monochromatic radiation. An alternative approach is provided using semiconductor detectors with white radiation (Bordas et al. 1976, Bordas and Randall 1978).

With a single fixed detector the whole scattering pattern can be recorded with good resolution. By displacing the detector, data can be collected to make the necessary absorption corrections.

Unfortunately, this technique is limited at present by the speed of the data acquisition systems. Developments in electronics would certainly give new impetus to this very elegant technique which makes optimal use of the wavelength continuum of SR. The availability of such a detector would open the way to many new experiments. Among them, fluctuation scattering is worth mentionning. A theory was proposed (Kam, 1977) based on the fact that particles in solution are free to rotate. The statistical fluctuations from the isotropic symmetry will result in fluctuations of the scattered intensity around the values of the averaged axially symmetric pattern.

These fluctuations can be processed by correlation analysis. Accumulation of the spatial correlation which is the average of the products of scattered intensities in two directions: $C(s1,s2) = \langle I(s1).I(s2)\rangle$, as a function of the scattering vectors s1 and s2 enhances structural information. In principle, the structure can be reconstituted from the spatial correlation using existing algorithms (Kam 1980). Feasibility studies using monochromatic radiation with a frozen solution of tobacco mosaic virus, to expand the time scale, gave encouraging results (Kam et al. 1981).
Other approaches to the use of polychromatic SR for solutions have been proposed (Stuhrmann,1978, Stamatoff, 1979) but have not yet been implemented. Further, the new impetus given to high resolution measurements offering a possibility of overlap between optical and electron microscopy and small angle scattering methods should lead to new information about large structures. This technique is also complementary to thermal neutron small angle scattering.

4.5.2. Physical and Chemical applications.

4.5.2.1. Alloys.

Naudon et al. (1979) have studied the distribution of concentration heterogeneities in aluminium alloys. Figure 24 illustrates the difference between the small angle scattering pattern of pure aluminium and that of a Al-Zn(6.8%) alloy. This work provides a good example of efficient use of SR: The data obtained at very low angles making use of the good collimation of SR were merged with the higher angle measurements made on a laboratory source to obtain a complete scattering pattern. A comparison with similar experiments using neutrons showed that , in this particular case, SR was a more efficient method both in terms of resolution and speed of data collection.
The good collimation of SR allowed Allain et al. (1980) to characterize oxydized particles which form in copper alloys undergoing internal oxydation. With $\mathcal{A} = 5 \cdot 10^{-3} \, \mathring{A}^{-1}$ the resolution was 10 times higher than with a standard camera.

The tunable character of SR can be a distinct advantage in the study of alloys as shown by the work of Flank et al.(1979) on amorphous alloys. By an appropriate choice of wavelength the fluorescence of elements like Fe and Ti could be minimized thus improving the signal to noise ratio.

4.5.2.2. Colloidal systems.

Ferrofluids.

Ferrofluids are colloidal suspensions of monodomain magnetic particles (e.g. cobalt, ferrite) with dimensions smaller than a few hundred Angstroms, in non magnetic fluids (e.g. organic solvents). There are an increasing number of technological applications of ferrofluids for instance in instrumentation. Anthore et al. (1979, 1980) have investigated the behaviour of ferrofluids in alternating magnetic fields. The field was switched on and off and the data were stored in separate parts of the memory of the acquisition system. Figure 25 illustrates the difference in the scattering pattern of a ferrite

ferrofluid in the presence and absence of a magnetic field. Here again, the tunability of the source – the measurements were carried out at $\lambda =$ 1.8 $\AA$- was a key factor in the success of the experiments.

Gels and sols.

Interesting studies on the swelling mechanism of Na-Montmorillonite (clay) gels have been carried out by Rousseau et al. (1979). Gels were first cooled to liquid nitrogen temperature and slowly heated. Careful thermal control of the sample showed that the pathway followed during this process is independent of the number of cooling cycles but that the final state depends on the exact nature of the initial state. The possibility to carry out such measurements in a routine fashion allows systematic studies of the parameters which influence the behaviour of these systems. (e.g. solvent, charge on the layers, concentration,etc.)

Bottero et al. (1979) have studied the structure of aluminium hydroxyde sols in an attempt to relate the ageing of the suspension and its

properties e.g. the absorbtion of colloids and detergents. Here again, the limited stability of the samples sets the requirement for the use of SR.

5. Other systems.

5.1. Partially ordered systems.

5.1.1. Introduction.

Until now, we have considered either very ordered or randomly oriented systems. These two extreme cases are the only ones for which a general theory is available.

For partially ordered systems (e.g. polymers and biological fibres) interpretation usually becomes extremely complex but can sometimes be facilitated by information supplied by other techniques, like electron microscopy.

A description of the methods used in these cases is well beyond the scope of this chapter and we will limit ourselves to a few examples where the use of SR has provided a real breakthrough. It should however be stressed once more that the impact that SR has had on all these fields comes not only from the availability of a new source, but also from the new approaches to detection,

data acquisition and data interpretation which the properties of the source are engendering.

Here again, we have, purely as a matter of convenience, separated the biological applications which are more numerous at present, from other studies.

5.1.2 Experimental techniques.

With very few exceptions studies on partially ordered systems make use of the high intensity of SR and only focusing and double focusing instruments provide enough flux to perform these experiments with monochromatic radiation. In some case, however, energy dispersive methods could be useful (see section 4.5.1.6). Initially, most SR X-ray cameras were specifically designed for studies on partially ordered systems (Barrington-Leigh and Rosenbaum, 1976; Haselgrove et al., 1977, Tchoubar et al., 1978, Holmes and Rosenbaum, 1980) whereas nowadays they are used for a broader range of applications (Bordas et al. 1980). The new requirements do not influence the X-ray optical system, except the beam path between

the sample and the detector, as much as the data acquisition systems.

5.1.3. Applications.

5.1.3.1 Synthetic polymers.

Traditionally, the study of the structure of
synthetic polymers has relied on systematic
studies requiring long exposures. Although the
rate of data acquisition can greatly be increased
by the use of SR and PSDs the advantage for static
measurements is much less obvious than in the case
of biological material since polymer samples are
usually stable.

As a result there have been, until now, relatively
few applications on polymers. Rault et al.
(1979) measured the long period of monodisperse
and polydisperse polyethylene , polypropylene and
1-polybutene obtained by quenching from the melt
with the aim to obtain a better description of the
crystallization process and to establish the
properties of polymer chains in the melt.

Progress in polymer applications of scattering
methods is however mainly to be expected from
studies of time dependent phenomena which are

difficult with conventional sources. The first
application of SR in this area was reported by
Koch et al.   (1981) who studied the kinetics of
crystallization of polyisobutylene after fast
stretching by monitoring the changes in intensity
of the characteristic 020 and 113 reflections in
the wide angle scattering pattern. The results
were interpreted using Avrami's equation and
showed that this crystallization process can be
interpreted as resulting from the athermal
formation of rods or fibrils.

Another example is provided by a study of the
decrease of the value of the long period with
crystallization time during the isothermal
crystallization of polyethylene terephtalate in
oriented (Elsner and Zachmann, 1979) and
unoriented samples (Elsner et al. 1980). Similar
measurements had been made using conventional
sources but the interpretation of the results was
not entirely clear since the samples had to be
quenched after various crystallization times and
the measurements were made at room temperature.

In the experiments at DORIS, the samples were
heated between 117°C and 145°C in an oven placed
directly in the path of the X-ray beam. The
crystallization process was followed continuously

at the crystallization temperature, the scattering curves being measured within 10 sec and 1 minute intervals. The time course of the scattering power Q $(Q=\int I(\mathcal{X}).\mathcal{K} d\mathcal{X})$ during crystallization is illustrated in figure 26. The results confirmed that the decrease of the long period with crystallization time is a genuine effect which can be explained by a decrease of the corrugation of the crystalline domains.

A similar, wide angle scattering experiment on melting of high density polyethylenes and polypropylenes was carried out in Novosibirsk (Forgacs et al. 1980).

5.1.3.2 Biological systems; Fibrous and lamellar systems.

Fibrous systems.

Fibrous systems usually consist of very anisotopic particles organized with their long axis parallel to the fibre axis. In most cases there is no azimuthal order and the scattering pattern corresponds to a cylindrically averaged structure. The diffraction patterns for those systems are most easily interpreted using cylindrical polar coordinates (r, ψ, z in real space, R, Ψ, Z in reciprocal space) for which the general expression of the structure factor is given by:

$$F(R, \Psi, Z) = \tag{68}$$
$$\int_0^\infty \int_0^{2\pi} \int_{-\infty}^\infty \rho(r, \psi, z) \exp\left\{ 2\pi i \left[R \cdot r \cos(\psi - \Psi) + zZ \right] \right\} r \, dr \, d\psi \, dz$$

When there is a repeat of c along the fibre axis as in the case of muscle the intensity is distributed along equally spaced layer lines at $Z = l/c$ where l is an integer. The structure factor is then given by:

$$F_l(R, \Psi, l/c) = \sum_{n=-\infty}^\infty F_{n,l}(R) \exp(i n \psi) \tag{69}$$

and

$$F_{n,\ell}(R) = exp \frac{i\,n\,\pi}{2} \int_0^\infty f_{n,\ell}(r) \, J_n\left(2\pi R \cdot r\right) 2\pi\,r\,dr \quad (70)$$

$$f_{n,\ell}(r) = \frac{1}{2\pi} \int_0^{2\pi}\!\!\int_0^c f_M(r, \psi, z) \, exp\left[\,i\left(n\psi - 2\pi\frac{\ell z}{c}\right)\right] d\psi\,dz \quad (71)$$

Where the Jn are the nth order Bessel functions and f_M (r,ψ,z) describes the electron density of the repeating unit. Details can be found in the textbook by Vainshtein (1966). The theory applies quite well for the interpretation of low resolution data. At higher angles interpretation is usually complicated by corrections which have to be applied to the experimental data to obtain the true intensity disribution in reciprocal space. A further complication arises from deviations from perfect axial order which mainly influence the pattern at higher angles.

Collagen exists in a variety of connective tissues which have very different structures.

Native rat tail tendon collagen,for instance, gives a very strong meridional diffraction pattern corresponding to a repeat of 670 Å. The latter results from fibrils which are 3000 Å long and staggered by 670 Å. The pattern has been studied in great detail using rotating anode sources and in the last ten years a fairly detailed structure has been obtained (Hulmes et al., 1977). SR has had its main impact in this field by allowing dynamic studies in which the mechanical properties of the fibres can be related to structural changes (Nemetschek et al. 1980a, Jonak et al. 1979, Nemetschek et al. 1980b). A typical example of the influence of chemical treatment on the scattering pattern is shown in figure 27. Further, information is presently being accumulated about the structure of less-ordered forms of collagen like cartilage and cornea. In cartilagenous tissue the collagen fibrils are embedded in a matrix of proteoglycans and glycosylaminoglycans. The samples are usually very poor scatterers which require several hours of exposure even using a double focusing camera. The X-ray studies on bovine intervertebral disc showed differences in the diffraction patterns from internal and external fibres (Berthet et al.

1979). Comparison of these patterns with the axial pattern of tendon and with patterns obtained from different types of reconstituted collagen should give information about the nature of the interaction between collagen and associated glycans which are still very unclear.

In the corneal stroma the collagen fibrils are of nearly uniform diameter and organized in lamellae. In each of the latter the fibrils have their axis oriented approximately parallel to each other, but not to those of neighbouring lamellae. Several theories have been proposed which attempt to relate the transparency of the cornea to the packing of the fibrils. Upon hydration, the tissue swells in the direction perpendicular to the plane of the lamellae and can take up more than 20 times its weight in water. The rate of this process which is accompanied by an increase in the average interfibrillar spacing is mainly dependent on the ionic strength of the swelling solution. (For a review on the properties of the cornea see Payrau et al. 1967) The packing of the fibrils gives a characteristic interference pattern which is being studied in detail using SR. One of the main features of the collagen diffraction pattern in cornea is the absence of a

strong first order which has not yet been completely explained. An interpretation of the axial electron density distribution in corneal collagen has been published recently (Heek et al. 1981). Experiments on this poorly scattering material can be routinely carried out on a double focusing camera where exposure times as short as 15 minutes give good quality patterns. Data has been obtained for fresh, dried and stained beef cornea. These results should give a better understanding of the organization of the constituents of cornea. A comparative study of material from different species should also be interesting since electron microscope studies have shown quite large differences between the corneas of different species. Figure 28 illustrates some typical scattering patterns obtained on this tissue.

Muscle; The mechanism of muscular contraction has been one of the most challenging problems in molecular biology for the last three decades. The study of this problem has been the main reason for the involvment of biologists in SR at a very early stage of its development. It should also be emphasized that most of the techniques for time resolved X-ray scattering (Faruqi and Huxley, (1978), Bordas et al. (1980)) have been developed in connection with this problem. This is interesting since it is one of the few cases, where techniques developed for the solution of a biological problem are later transferred to the study of physicochemical problems.

The model of muscular contraction which is generally accepted is one in which two partially overlapping arrays of protein filaments slides past each other, resulting in shortening of the muscle. The sliding is provided by crossbridges which project from the thick (myosin) filaments. The crossbridges attach to the thin (actin) filaments, swivel and detach. This process which repeats itself during contraction each time gives a displacement of approximately 150 Å. The model is general, although the relative position of the myosin and actin filaments differs considerably

from one type of muscle to another.

For instance in molluscan muscle they are organized in a rosette configuration consisting of a thick filament surrounded by 14 thin filaments. In vertebrate muscle the thick filaments lie in an hexagonal lattice on which the trigonal positions are occupied by the thin filaments. The characteristic layer-line pattern illustrated in figure 29 results from the regular helical arrangement of the crossbridges around the thick filaments.

Muscle studies have evolved along two main directions. Insect flight muscle, for which only small samples are available, have been used to obtain high resolution diffraction patterns in the rigor state as well as in the presence of unhydrolyzable nucleotide analogues. The relevance of these experiments depends on the assumption that the patterns in these two "frozen" states arise from two different conformations which may also occur during the contractile cycle of the myosin crossbridges. A detailed analysis of the results obtained sofar has been made by Holmes et al. (1980).

The second direction of research is represented by the time resolved measurements on vertebrate

(Huxley et al. 1980, Huxley et al. 1981a) and molluscan muscle (Lowy et al. 1979). Time resolutions of the order of 1 msec have been achieved in the case of vertebrate muscle, yielding the first direct experimental evidence of the motion of the myosin crossbridges during the contractile cycle. (Huxley et al. 1981b). It appears that during isometric contraction the intensity of the layer line pattern resulting from the ordered arrangement of the myosin crossbridges drastically decreases as tension increases and returns to its initial value when tension decays. A comparison of the time courses of the intensities and of tension shows that the structural changes preceed the tension changes by a few milliseconds.

The experimental time course of the 143 $\overset{o}{A}$ reflexion recorded with a linear position sensitive detector is illustrated in figure 30. It is hoped that time resolved diffraction measurements during more sophisticated mechanical experiments will give the direct experimental evidence required to prove or disprove the present model of muscular contraction. This would also have implications for the study of other contractile systems.

For DNA, the kinetics of transformation of the A to the B form has been studied. (Bram et al. 1979). Moreover, anomalous scattering techniques have been used to determine the localization of the metal ions in the cesium salt of DNA (Skuratovskii et al. 1980).

Lamellar systems.

Lamellar systems mainly occur in biological membranes and lipids which are their main constituents. The latter usually form highly polymorphic systems some of which have been well characterized using conventional sources (Tardieu et al. 1973). The phase transitions which occur in these systems are of considerable interest since similar phenomena may play a role in the function of biological membranes. Figure 31 shows characteristic scattering patterns and the corresponding arrangement of the lipids in egg lecithin (Ranck and Houdden, 1979). The kinetics of the phase transitions has been followed with a time resolution of the order of 10 msec for the stronger reflections using an X-ray temperature

jump device based on Peltier elements. It should be noted that these experiments are very demanding on the detector system as can be judged from the fact that one has to deal with a very inhomogeneous intensity distribution consisting of very narrow peaks with a considerable range of intensity which partly overlap during the phase transitions. Systematic investigations of the parameters which influence the transitions (concentration, length of the hydrocarbon chains etc.) are now required to understand these phenomena.

Another very interesting example of the application of SR to those systems is provided by the work of Stamatoff et al. (1979). These authors attempted to determine the position of metal atoms (Cu, Fe) associated with redox centres of hydrated oriented multilayers of biological membranes using anomalous scattering. In principle, it is possible to determine the position of the metal atoms within the membrane components both in the profile and in the membrane plane. The magnitude of the experimentally observed effects showed that significant results can be obtained at least for the metal atom distribution in the profile of the membrane.

5.1.3.3. Liquid crystals.

Liquid crystals consist of long rod-like molecules, typically containing two benzene rings in the centre and aliphatic hydrocarbons at each end. The rich variety of phases in liquid crystals, the description of which is beyond the scope of the present review, may be regarded as intermediate phases between the crystalline solid state and the isotropic liquid state (De Gennes, 1974). Very high momentum resolution in conjunction with high intensity are mandatory for accurate characterization of these phases and their transformations. To achieve adequate resolution the proper tool is a triple axis spectrometer installed at a SR source. An example of such an instrument is illustrated in figure 32 (Als-Nielsen, 1981). With perfect crystal monochromators and analyzer a momentum resolution of the order of 10^{-4} Å^{-1} is attainable as required for the measurement of correlation lengths of the order of 10^4 Å as found in liquid crystals. Experiments using this type of device have been performed by Moncton et al. (1980a, 1980b, 1981a) and by Christensen and Als-Nielsen (1981).

Comparison between the results obtained with freely-suspended films using a rotating anode tube and SR clealy show the advantage of the latter source (Moncton et al. 1980b).

5.1.3.4. Two-dimensional systems.

The atomic structure of surfaces and physisorbed monolayers may be studied by diffraction methods, and electron diffraction (LEED, THEED, RHEED) has proved to be a valuable method. However, the relatively short coherence length is a limiting factor and it is difficult to interpret measured intensities because the fundamental interaction is so strongly peaked around the forward scattering direction that multiple scattering contributes significantly to the scattering observed at intermediate and large angles. Another serious limitation is that the sample must always be in vacuum. These drawbacks do not exist with X-ray diffraction which also allows greater flexibility in sample environment. SR is especially suitable for this type of studies because of its high intensity and excellent collimation. Eisenberger

and Harra (1981) have studied reconstructed single crystal surfaces using the X-ray total external reflection Bragg diffraction (Harra, Eisenberger and Cho, 1979). In this method, a monochromatic X-ray beam is incident upon a surface at very glancing angles, typically less than $1°$. The incident beam can be both reflected out of the surface (total reflection) at small angles and diffracted parallel to the surface over large angles. This provides diffraction from the two-dimensional surface with little disturbance from the bulk crystal. The need for an intense source is twofold: The number of scattering atoms is exceedingly small and the Bragg scattering is not concentrated into spots but into rods perpendicular to the surface. A very good collimation is obviously needed in this case and provides good momentum resolution when a triple axis spectrometer of the type described in Section 5.1.3.3 is used. Eisenberger and Harra (1981) showed that the diffraction patterns obtained by this method can be interpreted without difficulty and that reliable results can be obtained even with a 60 kW rotating anode X-ray tube. However, identical experiments performed at SSRL have shown a 100-fold increase of integrated intensity. The

authors conclude that the relatively large signal means that a virtually unlimited variety of problems can be studied using the X-ray total external reflection Bragg diffraction method with SR.

Monolayers of noble gases (Kr, Ar) physiosorbed on graphite are other examples of two-dimensional systems which have received considerable attention recently. They have been studied using rotating anode tubes as well as SR. We only present the latter results here.

Certain graphite products (e.g. UCAR-ZYX) are composed of thin smooth flakes with the mean direction of the six-fold axis of the graphite crystallites perpendicular to the surface of the flake. In the plane of the layer the cristallites are oriented randomly and the spread of direction of the six-fold axis can be as large as 20°. Such flakes can have a large physisorbing surface area per unit volume. Due to the random orientation of the crystallites the adsorbed layers (e.g. of Kr or Ar) form a two-dimensional "powder".

In order to measure the diffraction pattern of this two-dimensional "powder" the sample is placed on the spectrometer with the layers parallel to the scattering plane. This leads to a diffraction pattern like the one illustrated in figure 33.

The sharpness of the Bragg peak gives the coherence length. However, the high wavevector side of the "Bragg peak" is intrinsically broadened in a two-dimensional "powder" (Warren, 1941) so that the coherence length is actually determined by the sharpness of only the low wavevector side of the "Bragg peak". In order to measure the sharpness a very high momentum resolution is required. As illustrated in figure 33 the coherence length in the case of Kr at 90°K is 2000 Å and thus, momentum resolution has to be better than $5 \ 10^{-4} \ \text{Å}^{-1}$

This has been achieved using SR with a triple axis spectrometer of the type shown in figure 32. Results on these systems were reported by Birgenau et al. (1981), Honcton et al.(1981b), Nielsen et al. (1980) and Nielsen et al.(1981).

The physics of condensed matter in two dimensions is of fundamental interest in itself (e.g. melting in two-dimensions) but it may also play an important role in the interpretation of phenomena in the technology of catalysts or membrane biology.

5.2. Disorder in ordered systems.

The structure of the one dimensional organic metal $(TTT)_2 I_3$ (bis-tetrathiotetracene-triiodine) was studied as a function of temperature and iodine concentration (Megtert et al. 1979) using a fixed film, fixed crystal, monochromatic technique. The diffraction pattern is formed by the superposition of a first pattern consisting of the weak Bragg reflections corresponding to the 3D ordered TTT sublattice and a second one with intense diffuse lines resulting from the interaction of the Ewald sphere (see section 1.5.2) with diffuse sheets. Robin et al.(1980) used SR in their study of the solid state polymerisation mechanism and phase transitions of a diacetylene. The observation of diffuse scattering gave a proof that polymerization proceeds homogeneously inside the monomer crystal. The high intensity of SR is a major asset for the study of weak effects which can change rapidly during chemical reactions or phase transitions.

Conclusion.

The progress made in the use of scattering methods with SR during the last few years is most strikingly illustrated by a look back at the "blue books" describing the European Synchrotron Radiation Facility project (Farge and Duke, 1979). Most of the topics related to X-ray scattering mentionned in this collective view on the future have now become very active research fields.
The use of X-ray scattering methods with SR was largely pioneered by biophysicists who were mainly in search of a brighter source to study phenomena in poorly scattering biological samples. The situation rapidly changed when they were joined by scientists from very different horizons but who, for the large majority, had already been involved in neutron scattering.
As a result the other natural properties of SR i.e. the smooth wavelength distribution and the high collimation are being increasingly used. The application of polarization and time structure have, however, not yet been seriously explored for elastic scattering experiments. A brief survey will show the extent of the evolution.

Protein crystallographers are now routinely collecting data on storage rings and feasibility studies for kinetic experiments are under way. For these studies, high intensity, wavelength tunability and good collimation are the major assets of SR.

Many former sceptics in this area of structural research which has well established traditions have turned into assiduous users of the new sources.

Another example is provided by the rapidly growing interest of polymer physicists and metallurgists after the first few time resolved small angle scattering and diffraction studies which have been performed. There is an increasing demand for dedicated instruments for this type of work which is also backed by industrial research groups.

Time-resolved X-ray scattering techniques in biology are routinely used not only for fibres but increasingly also for the study of systems in solution. Here again, the field has already developed to the point that one can contemplate much more sophisticated experiments (e.g. magnetic orientation of biomolecules).

Anomalous small angle scattering techniques have been explored and one can realistically consider

their use to solve structural problems in biology, metallurgy and polymer science.

The first powder diffraction studies with SR have shown an incresed resolution as a result of the good collimation, which should allow to solve larger structures than has hitherto been the case. Further, the high intensity enables measurements under extreme conditions e.g. high pressure in times of the order of minutes i.e. short enough to envisage routine application of these methods. Studies on liquid crystals and on systems with two-dimensional order have gained considerably from the use of SR both in resolution and speed of data collection. The same considerations apply obviously to ultra small angle scattering studies on biological material which would not be feasible without SR.

On the other hand, already established fields like topography or crystal optics have continued a more steady, if somewhat less spectacular growth as can be judged from the recent literature. Recent developments in interferometry are especially interesting. Experiments are also becoming more elaborate e.g. by the use of stroboscopic methods in topography. Further progress here is, however, already often limited by the quality of the

available sources as opposed to the situation in protein crystallography and time resolved measurements where the immediate difficulties still lie in the development of appropriate ancillary equipment and especially detectors.

These two effects combine to explain why the determination of accurate electron densities is the only topic mentionned in the "blue books" where no progress seems to have been made. These experiments require extremely accurate measurements which are presently limited by the stability of the sources and the response of the detectors.

Similarly, extension of white beam methods to a wider range of applications although shown by feasibility studies to be potentially extremely useful, depends on the development of appropriate energy dispersive detectors.

In view of the flourishing of papers in recent years one has many reasons to be optimistic about the future development of X-ray diffraction methods with synchrotron radiation. It is clear from the evolution that one is rapidly reaching the steep part of the growth curve especially as new dedicated sources become available in all parts of the world.

TABLE I
X-RAY DIFFRACTION METHODS FOR STRUCTURAL STUDIES

Incident beam	Monochromatic $\lambda = \lambda_0 =$ constant	Polychromatic $\theta = \theta_0 =$ constant
Bragg equation	$2d_{HKL} \sin\theta_{HKL} = \lambda_0$	$2d_{HKL} \sin\theta_0 = \lambda_{HKL} = ch/E_{HKL}$
Powdered crystal ●		
Single crystal ● — Fixed	(legend: ⊙ Source of monochromatic X-rays; ✵ Source of polychromatic X-rays; ‖ Collimators; ⊃ X-ray detector; ■ X-ray semiconductor detector; M.P.H.A. Multichannel pulse height analyzer)	large area detector
Single crystal ● — Rotating		

For references see text

TABLE II
INTEGRATED INTENSITIES FORMULAE FOR X-RAY DIFFRACTION METHODS FOR STRUCTURE STUDIES (KINEMATICAL APPROXIMATION)*

Sample \ Incident beam	Monochromatic $\lambda = \lambda_0$	Polychromatic $\theta = \theta_0$
Powdered crystal	$j'i_0(\lambda_0)\Delta\lambda_0 \frac{V}{v_0^2} |F|^2 \lambda_0^3 \frac{p}{4\sin\theta}$	$j'i_0(\lambda) \frac{V}{v_0^2} |F|^2 \lambda^4 \frac{p\cos\theta_0 \Delta\theta_0}{4\sin\theta_0}$
Single crystal — Fixed	No integrated intensity measurements possible	a. Small area detector – one direction in momentum space. b. Large area detector – certain volume of momentum space $i_0(\lambda) \frac{V}{v_0^2} |F|^2 \lambda^4 \frac{p}{2\sin^2\theta_0}$
Single crystal — Rotating	$j''i_0(\lambda_0)\Delta\lambda_0 \frac{V}{v_0^2} |F|^2 \lambda_0^3 \frac{p}{2\pi\sin 2\theta}$	$j'''i_0(\lambda) \frac{V}{v_0^2} |F|^2 \lambda^4 \frac{p\Delta\theta_0}{4\pi\sin^2\theta_0}$

* Buras and Gerward 1975.

References.

Aggerbeck, L., Pernot, P., Ranck, J.L. and
Tardieu, A., 1981, Rapport d' activite, L.U.R.E.,
Universite Paris-Sud, p III-24

Allain, J. Haudon, A. and Caisso, J., 1980, Ann.
Chim. Fr.,5, 49.

Als-Nielsen, J.,1981, Risø National Laboratory
Report N-2268.

Anomalous Scattering. eds. Ramaseshan, S. and
Abrams, S.C., 1975, Munksgaard: Copenhagen.

Anthore, R., Gauthier,S. Lemonnier,M., Lissalde,
F.,Martinet,A., Petitpas, C. and Rousseaux, F.,
1979, Rapport d' activité, L.U.R.E., Université
Paris-Sud, p 80.

Anthore, R., Gauthier, S., Martinet, A. and
Petitpas, C., 1980, I.E.E.E. Trans. Mag. MAG.,
16, 197

Arndt, U.W., 1978, Nucl. Instr. and Meth., 152,
307.

Arndt, U.W. and Gilmore, D.J., 1979, J. Appl.
Cryst., 12 ,1.

Authier, A., 1977, in "X-Ray Optics" Ed. H.-J.
Queisser, Topics in Appl. Physics, Vol. 22 pp
145-189, (Springer Verlag: Berlin)

Azaroff, L.V., Kaplow, R., Kato, N., Weiss, R.J.,
Wilson, A.J.C. and Young, R.A., 1974, X-Ray
Diffraction, Mc Graw-Hill Inc.: New York.

Bacon, G.E., 1966, X-Ray and neutron diffraction,
Pergamon Press: London.

Barrington-Leigh, J. and Rosenbaum, G., 1976, Annu. Rev. Biophys. Bioeng. 5, 239.

Bartels, K., 1981, J. Appl. Cryst. (in press)

Bartunik, H.D., Bartels, K., Fourme, R., Kahn, R., Andre, D. and Gadet, A. , 1979, Collected Abstracts, European Crystallography Meeting, ECM5, Copenhagen.

Bartunik, H.D., Clout, P.N., Robrahn, B., 1981, J. Appl. Cryst. 14, 134

Bartunik, H.D., Fourme, R. and Phillips, J.C., 1982, in "Uses of Synchrotron Radiation in Biology" Ed. Stuhrmann, H.B., Academic Press: London.

Bartunik, H.D. and Schubert, P., 1981, J. Appl. Cryst. (in press)

Bartunik, H.D., Jerzembek, E., Pruss, D., Huber, G. and Watson, H.C., 1981, Abstracts, IUCr Meeting, Ottawa.

Baru, S.E., Proviz, G.I., Savinov, G.A., Sidorov, V.A., Feldman, I.G. and Khabakhphasev, G.A., 1978, Nucl. Instr. and Meth., 152, 195

Benedict, U., Buras, B., Gerward, L., Olsen, S.J. and Steenstrup, S., 1980, private comm.

Berthet-Colominas, C., Tochetti, D., Miller, A., Bordas, J. and Koch, M.H.J., 1979, EMBO-EMBL workshop on "X-ray and neutron scattering of biological stuctures" Hamburg 24-28 september.

Birgenau, R.J., Brown, G.S., Horn, P.M., Moncton, D.E. and Stephens, P.W., 1981, J.Phys. C 14, L49.

Blow, D.M., 1958, Proc. Roy. Soc., A247, 302.

Blundell, T.L. and Johnson, L., 1976, Protein Crystallography (Academic Press: London)

Bonse, U. and Graeff, W., 1977, in "X-ray Optics", Ed. Queisser, H.J., Topics in Appl. Phys. Vol 22. pp 93-143 (Springer Verlag: Berlin)

Bonse, U. and Hart, M., 1965, Appl. Phys. Lett., 6, 155.

Bonse, U. and Hart, M., 1966, Z. Physik, 189, 151

Bonse, U. and Materlik, G., 1975, Acta Cryst. A31, 232

Bonse, U. and Materlik, G., 1976, Z. Physik B24, 189

Bonse, U., Spieker, P., Hein, J.T. and Materlik, G., 1980, Nucl. Instr. and Meth., 172, 223.

Bonse, U.and Fisher, R. (1981) DESY report SR/OOO (in press)

Bordas, J., Glazer, A.M. and Hauser, H., 1975, Phil. Mag., 35, 1257

Bordas J., Munro I.H. and Glazer A.M., 1976, Nature 262, 541

Bordas J. and Randall J.T., 1978, J. Appl. Crystallogr. 11,434

Bordas, J., Koch, M.H.J., Clout, P.N., Dorrington, E., Boulin,C., and Gabriel, A., 1980, J.Phys.E. 13, 938

Bottero, J.Y., Tchoubar, D., Rousseaux, F., 1979, Rapport d'Activité, L.U.R.E., Université

Paris-Sud, p 83.

Bragg, W.L., 1913, Proc. Cambridge Phil. Soc. 17, 43.

Bragg, W.L., 1914, Phil. Mag. 28, 355.

Bram ,S., Rimsky,A., Laigle,A., Lelacvivier,H., Froussart,P., 1979, Rapport d'activité, L.U.R.E., Université Paris-Sud,p 53.

Brunel, H. and de Bergevin, F., 1981, Acta Cryst.,A37, 324.

de Bergevin, F. and Brunel, H., 1981, Acta Cryst., A37, 314.

Brunel, H., Patrat, G., de Bergevin, F., Rousseau, F. and Lemonnier, M., 1979, Rapport d' activité, L.U.R.E. , Université Paris-Sud

Buckley-Golder, I.M., Tanner, B.K. and Clark, G.F., 1977, J. Appl. Cryst. 10, 502.

Buras, B. and Gerward, L., 1975, Acta Cryst. A31, 372, and references therein.

Buras, B., Olsen, S.J., Gerward, L., Will, G. and Hinze, E., 1977, J. Appl. Cryst. 10, 431.

Buras, B., Olsen, S.J. and Gerward, L.,1978, Nucl. Instr. and Meth. 152, 293.

Buras, B., 1980, National Bureau of Standards Special Publication 567, p. 33 and références therein.

Buras, B., Olsen, S.J. and Gerward, L., 1980a, and Nucl. Instr. and Methods 178, 131

Buras, B., Cox, D., Gerward, L., Olsen, S.J. and

Steenstrup, S., 1980b, private comm.

Charpak, G., Sauli, F. and Kahn, R., 1978, Nucl. Instr. and Meth., 152, 185

Chikauba, Y. and Tanner, B.K., 1979, Jap. J. Appl. Phys., 18, 1389

Christensen, F. and Als-Nielsen, J.,1981, (to be published)

Clark, G.F., Tanner, B.K., Sery, R.S. and Savage, H.T., 1979, J. de Physique, 40,C5-183.

Cohen, G.G. and Kuriyama, H., 1978, Phys. Rev. Letters, 14, 40.

Compton, A.H. and Allison, S.K., 1935, X-rays in Theory and Experiment p 39, Van Nostrand: New York.

Cotton J.P. and Benoit, H., 1975, J. Phys. 36, 905.

de Bergevin, F. and Brunel, H., 1972, Phys. Lett., 391, 141.

Debye, P., 1915, Ann. Physik, 46,809.

De Gennes, P.G., 1974, The Physics of Liquid Crystals, (Clarendon Press:Oxford)

Dessen, Ph., Blanquet, S., Gulik, A., Le Maire, M., Tardieu, A. and Vachette P., 1979, Rapport d'activité. L.U.R.E., p 51, Université Paris-Sud.

Elsner, G. and Zachmann, H.G., 1979, DESY SR-79/18

Elsner, G., Koch, M.H.J., Bordas,J. and Zachmann, H.G., 1981, Makromol. Chem. , 182, 1263.

Farge, Y. and Duke, P.J.,Eds. 1979, "European Synchrotron Radiation Facility - Feasibility study" European Science Foundation,Strasbourg.

Faruqi, A.R. and Huxley, H.E., 1978, J. Appl. Cryst. 11, 449

Feil, D., 1977, Isr. J. Chem. 16, 103.

Flank, A.M., Haudon,A. and Caisso, J., 1979, Rapport d' activité, L.U.R.E., Université Paris-Sud, p 79.

Fourme, R., 1979, in "Synchrotron Radiation Applied to Biophysical and Biomedical Research" p 349 Eds. Castellani, A. and Quercia, I.F., (Plenum Press:New York)

Freund, A., 1975, in "Anomalous scattering", Eds. Ramaseshan,S. and Abrahams, S.C., (Munksgaard: Copenhague)

Friedrich, W., Knipping and Laue, M., 1912, Proc. Bavarian Acad. Sci., 303

Forgacs, P., Shermonov, H.A., Tolochko, P., Mezentsev, H.A. and Pindurin, V.F., 1980, J. Polym. Sci. Polym. Phys., 18, 2155.

Gabriel, A., 1977, Rev. Sci. Instrum. 48,1303

Gabriel, A., Dauvergne, F. and Rosenbaum, G., 1978, Nucl. Instr. and Methods, 152, 191

Gastaldi, J. and Jourdan, G., 1978, Phys. Stat. Sol. (a) 49, 529

Gastaldi, J. and Jourdan, G., 1979, Phys. Stat. Sol. (a) 52, 139

Graeff, W. and Bonse, U., 1977, Z. Phys.,B27, 19

Graeff, W., 1981, (private communication)

Green, D.W., Ingram, V.H. and Perutz, H.F., 1954,
Proc. Roy. Soc., A225, 287

Guinier A. and Fournet G., 1955, Small angle
scattering of X-rays. (John Wiley: New York)

Guinier, A. and Tennevin, J., 1949, Acta Cryst.
2, 133

Harmsen, A., Leberman, R. and Schulz, G.E., 1976,
J. Mol. Biol. 104, 311

Hart, H., 1975, J. Appl. Cryst., 8, 436

Hart, H., 1978, Phil. Mag., B38, 41

Hart, H. and Lang, A.R., 1961, Phys. Rev.
Letters, 7, 120

Hart, H. Sauvage, H. and Siddons, D.P. (1980)
Acta Cryst., A36, 947.

Hartmann, W., 1977, in "X-Ray Optics", Ed. H.-J.
Queisser, Topics in Appl. Phys. Vol. 22, pp
191-219 (Springer Verlag: Berlin).

Hartt, J. and Mendelson, R.A., 1979, Biophys. J.
25, 20a

Haselgrove, J.C., Faruqui, A.R., Huxley, H.E. and
Arndt, U. W., 1977, J. Phys. E., 10, 1035.

Hastings, J.B., Kincaid, B.H. and Eisenberger,
P.,1978, Nucl. Instr. and Methods, 152, 167

Helliwell, J.R. and Worgan, J.S., 1981, J. Appl.
Cryst., 000,000

Hendrix, J., Koch, M.H.J. and Bordas, J., 1979,

J. Appl.Cryst., 467.

Herzenberg, A. and Lau, H.S.M., 1967, Acta Cryst. 22, 24

Hinze, E. and Huding, A., 1980, private comm.

Hoppe, W. and Jakubowsky, U, 1976, in Anomalous Scattering, Eds. Ramaseshan, S. and Abrahams, S.C. p 437, (Munksgaard: Copenhague)

Holmes, K.C. and Rosenbaum, G., 1979, In Synchrotron Radiation Research, p XXX Eds. Doniach, S. and Winick, H. (Plenum Press: New York)

Holmes, K.C., Tregear, R.T. and Barrington Leigh,J., 1980, Proc. R. Soc. Lond. B 207, 13

Hulmes, D.J.S., Miller,A., White, S.W. and Doyle,

B.B., 1977, J. Mol. Biol. 110, 643.

Huxley ,H.E., Faruqi, A.R., Bordas,J., Koch, M.H.J. and Milch, J., 1980, Nature 284,140.

Huxley, H.E., Faruqi, A.R., Kress, M., Bordas, J. and Koch, M.H.J., 1981a, J. Mol. Biol, (in press)

Huxley, H.E., Simmons, R.M., Faruqi, A.R., Kress, M., Bordas,J. and Koch, M.H.J. , 1981b, Proc. Natl. Acad. Sci. USA 78, 2297.

International Tables for X-ray Crystallography , 1962, Vol III, (Birmingham: Kynoch Press)

Ibel, K. and Stuhrmann, H.B., 1975, J. Mol. Biol., 93, 255.

James, R.W., 1962, The Optical Principles of the

Diffraction of X-rays (Bell and Sons Ltd: London)

Jonak, R., Hemetschek-Gansler, H., Hemetschek, Th.,Riedl, H., Bordas, J. and Koch, H., 1979, J. Mol. Biol., 130,511.

Jourdan, C. and Gastaldi, J., 1979, Scripta Met., 13, 55

Kahn, R., Fourme, R., Caudron, B., Bérard, R., Benoit, R., Bouclier, R., Charpak, G., Santiard, J.C. and Sauli, F. (1980) Nucl. Instr. and Methods, 172,337.

Kalman, Z.,1979, Acta Cryst.,A35,634.

Kam, Z., 1977, Macromolecules, 10, 927.

Kam, Z., 1980, J. Theor. Biol. 82, 15.

Kam, Z., Koch, M.H.J. and Bordas, J., 1981, Proc. Natl. Acad. Sci. USA, 78, 3559.

Karabekov, I.P., Egikian, D.I., Mikaelyan, R.A., Bagdasarian, J.G. and Datsenko, L.I., 1977, Yerevan Institute of Physics, preprint 258(51)

Koch M.H.J., Parfait R.,Haas J.,Crichton, R.R. and Stuhrmann H.B., 1978, Biophys. Struct. Mechanism 4,251.

Koch M.H.J., Bordas J. Schöla E. and Broecker H. Chr. Polymer Bull., 1979, 1, 709.

Koch, M.H.J., Stuhrmann, H.B., Tardieu, A. and Vachette, P., 1981, in "Uses of synchrotron radiation in biology" Ed. H.B. Stuhrmann, (Academic Press: London) in press.

Kohra, K., Matsushita, T., Ishida, H. and Ishikawa, T., 1978, XIth Int. Congr.

Crystallogr., Abstract 11.2-26, S257, Warsaw.

Kronig, R. de L. and Kramers, H.A. 1928, Z.
Physik 46, 174

Kruse, J., Witz, J. and Tardieu, A., 1981,
Rapport d'activite L.U.R.E., Universite Paris-Sud,
p III-22

Laine, E. and Lahteenmaki, 1980, J. Mat.
Science, 15, 269.

Lang, A.R., 1959, Acta Cryst. 12, 249.

le Maire, M., Möller, J.V. and Tardieu, A., 1981,
J. Mol. Biol. in press.

Lemonnier, M., Fourme,R., Rousseaux, F. and
Kahn,R., 1978, Nucl. Instr. and Methods, 152,
173.

Letellier, L., Schechter, E., Ranck, J.L.,
Tardieu, A. and Pernot, P., 1981, Rapport d'
activité, L.U.R.E., Université Paris-Sud, p
III-25.

Lissalde, F., Gauthier, S. and Puget, R., 1979,
Rapport d'activité, L.U.R.E., Université
Paris-Sud.

Lowy, J., Poulsen, F.R. ,Bordas,J. and
Koch,H.H.J., 1979, EMBO-EMBL workshop on "X-ray
and neutron scattering of biological structures "
Hamburg 24-28 september.

Luzzati V. and Tardieu A., 1980, in "Ann. Rev.
Biophys. Bioeng." (ed. Mullins) Ann. Revs.
Inc: Palo Alto, Calif.

Lye, R.C., Phillips, J.C., Kaplan, D., Doniach, S.
and Hodgson, K.O., 1980, Proc. Natl. Acad. Sci.
USA 77, 5884

Mac Cormack, I.B. and Tanner, B.K. , 1978, J. Appl. Cryst. 11, 40.

Manghnani, M.H., Skelton, F.E., Ming, L.C., Qadri, S. and Balogh, J., 1981, Proc. of the International Symposium on the Physics of Solids under High Pressure, Bad Honnef, West Germany, August 10-14, 1981 (in press).

Mandelkow E., Harmsen A., Mandelkow E.M. and Bordas J., 1980, Nature, 287, 595.

Marra, W.C., Eisenberger, P. and Cho, A.Y., 1979, J. Appl. Phys. 50, 6927.

Marshal, W., and Lovesey, S.W., 1971, "Theory of thermal neutron scattering" (Clarendon Press: Oxford)

Mathieson, A. McL., 1977, Acta Cryst., A33, 133.

Materlik, G., 1981, Proc. of the Workshop on Neutron Interferometry, Ed. by Bonse, U. and Rauch, H., p 431, (Oxford University Press:)

Megtert, S., Pouget, J.P. Comes, R. and Fourme, R., 1979, in Quasi one-dimensional conductors II, p 196, Lecture Notes in Physics Nr 96 (Springer Verlag: Berlin).

Meek, K.M., Elliott, G. F., Sayers, Z., Whitburn, S.B. and M.H.J. Koch, 1981, J. Mol. Biol. 149, 477.

Miltat, J., 1980, In Imaging processes and Coherence in Physics, p 503, Lecture Notes in Physics Nr 112, (Springer Verlag: Berlin).

Miltat, J., 1981,in "Characterization of Crystal growth defects by X-ray methods" (Plenum Press:

New York)

Miltat, J. and Bowen, 1979, J. de Physique, 40, 389.

Miltat, J. and Dudley, M., 1980, J. Appl. Cryst. 13, 555.

Miltat, J. and Kleman, 1979, J. Appl. Phys., 50, 7695.

Molinari, A., 1980, Physics Reports 64, 283.

Moliere, G., 1939, Ann. Phys., 35, 272

Moncton, D.E., Pindak, R. and Brown, G.S. 1980a, (to be published)

Moncton, D.E., Pindak, R., 1980b, in "Ordering in

Two Dimensions", S.K. Sinha, Ed.., p83 (North Holland: Amsterdam)

Moncton, D.E., Persham, P.S. and Als-Nielsen, J., 1981a, (in press)

Moncton, D.E., Stephens, P.W., Birgenau, R.J., Horn, P.M. and Brown, G.S., 1981b, Phys. Rev. Lett. 46, 1533.

Moody, M.F., Vachette P. and Foote, A., 1979, J. Mol. Biol. 133,517.

Moody M., Vachette P., Foote A., Tardieu A.,Koch M.H.J. and Bordas J., 1980, Proc. Natl. Acad. Sci. USA 77, 4040.

Naudon, A., Allain, J. and Himault,J., 1979, Rapport d' activité, L.U.R.E. Université Paris-Sud p 79

Haudon, A., Lemonnier, H. and Rousseaux, F., 1979, C.R. Acad. Sci. Paris, 288, série L, 21

Hemetschek, Th., Riedl, H., Jonak,R., Hemetschek-Gansler, H., Bordas, J. and Koch, H.H.J., 1980a, Virchows Arch. A. Path. Anat. and Histol. 386, 125.

Hemetschek, Th., Jonak, R., Hemetschek-Gansler, H., Riedl, H., Schilling, V., Bordas, J. and Koch, H.H.J., 1980b, Naturwiss., 67, 416.

Nielsen, H, Als-Nielsen,J. and Mc Tague, J.R., 1980, in Riso National Laboratory Report M-2268

Nielsen, H., Als-Nielsen, J., Bohr, J. and Mc Tague, J.P., 1981, (to be published)

Olsen, S.J., Buras, B., Gerward, L., Johansson, B., Lebech, B., Skriver, H. and Steenstrup, S., 1981a, Proc. of the International Symposium on

the Physics of Solids under High Pressure, Bad Honnef, West Germany, August 10-14, 1981 (in press)

Olsen, S.J., Buras, B., Gerward, L. and Steenstrup, S., 1981b, J. Phys. E., (in press)

Parrish,W. and Erickson, C.G., 1978, XIth Int. Congr. Crystallogr., Abstract 14.2-3 p 5331, Warsaw.

Payrau, P., Pouliquen, Y., Faure, J.P. and Offret, G., 1967, La transparence de la cornee, (Masson et Co.: Paris)

Petroff, J.F. and Sauvage, M., 1978, J. of Crystal Growth, 43, 628.

Petroff, J.F., Sauvage, M., Riglet, P. and Hashizume, H., 1980, Phil. Mag. A, 42, 319.

Phillips, J.C., 1078, Ph. D. Thesis, Stanford University, USA.

Phillips, J.C., Cerino, J.A. and Hodgson, K.O., 1979, J. Appl. Cryst., 12, 592

Phillips, J.C. and Hodgson, K.O., 1980, Acta Cryst., A36, 996

Phillips, J.C., Templeton, D.H., Templeton, L.K. and Hodgson, K.O., 1978, Science, 201, 257

Phillips, J.C., Wlodawer, A., Yevitz, M.H. and Hodgson, K.O., 1976, Proc. Natl. Acad. Sci. USA, 73, 128

Phillips, J.C., Wlodawer, A., Goodfellow, J.M., Watenpaugh, K.D., Sieker, L.C., Jensen, L.H. and Hodgson, K.O., 1977, Acta Cryst. A33, 445

Phizackerley, R.P., Cork, C.W., Hamlin. R.G., Nielsen, C.P., Vernon, W., Xuong, N.H., and Perez-Mendez, V., 1980, Nucl. Instrum. and Meth., 172, 393.

Platzman, P.M. and Tzoar, N., 1970, Phys. Rev. 132, 3556.

Post, B. , 1977, Phys. Rev. Lett. 39, 760.

Pouget, J.P., Megtert, S., Comes, R. and Epstein, A.J., 1980, Phys. Rev. B21, 486

Prober, J.M. and Schultz, J.M., 1975, J. Appl. Cryst., 8, 405.

Raman, S., 1959, Proc. Ind. Acad. Sci., 50A, 95

Ranck J.L. and Moudden, H., 1979, Rapport d'activité, L.U.R.E. Université Paris-Sud, p 52.

Rault, J., Robelin, E., Rousseau, F., Lemonnier, M., 1979, Rapport d' activité, L.U.R.E. , Université Paris-Sud, p 84

Riglet, P., Sauvage, M., Petroff, J.F. and Epelboin, Y., 1980, Phil. Mag. A, 42, 339.

Rietveld, H.M., 1969, J. Appl. Cryst., 2, 65.

Ruoff, A.L., 1981, Proc. of the Internatiaonal Symposium on the Physics of Solids under High Pressure, Bad Honnef, West Germany, August 10-14, 1981 (in press)

Robin, R., Pouget, J.P., Comes, R. and Moradpour, A., 1980, J. de Phys. 41, 415.

Rousseau, F., Pons ,C.H., Tchoubar,D. and Lemonnier, M., 1979, Rapport d' activité, L.U.R.E., Université Paris-Sud,p 82.

Safa, M. and Tanner, B.K., 1978, Phil. Mag., B37, 739

Sauvage, M., 1978, Nucl. Instr. Methods, 152, 313

Sauvage, M., 1981, in "Characterization of crystal growth defects by X-ray methods" (Plenum Press: New York)

Sauvage, M., Petroff, J.F. and Skalicky, P., 1977, Phys. stat. sol. (a) 43, 473.

Sauvage, M., Malgrange, C., Petroff, J.F. and Skalicky, P., 1979, Rapport d'Activité, L.U.R.E., Université Paris-Sud

Sauvage, M. and Petroff, J.F., 1980, in Synchrotron Radiation Research, p 607, Eds. Winick, H. and Doniach, S. (Plenum Publishing Co: New York)

Schulz, L.G., 1954, Trans. AIME, 200, 1062.

Sery, R.S., Savage, H.T., Tanner, B.K. and Clark, G.F., 1978, J. Appl. Phys., 49, 2010

Skalicky, P. and Malgrange, C., 1972, Acta Cryst., A28, 501

Skelton, F., 1980, private comm.

Skuratovskii, I.Ya., Volkova,L.I., Kapitonova, K.A. and Bartenev,V.N., 1980, J. Mol. Biol. 134, 369

Stamatoff, J.,1979, Biophys. J., 26,325.

Stamatoff J., Eisenberger P., Brown G., Pachence J., Dutton L.,Leigh J. and Blasie K., 1979,

Biophys. J., 25 44a

Steinberger, I.,T., Bordas, J. and Kalman, Z.H., 1977, Phil. Mag., 35, 1257

Stephenson, J.D., Kelha, V., Tilli, H. and Tuomi, T., 1978, Nucl. Instr. and Methods, 152, 319

Stephenson, J.D., Kelha, V., Tilli, H. and Tuomi, T., 1979, Phys. Stat. Sol.(a), 53, 571

Stewart, R.F. and Feil, D., 1980, Acta Cryst., A36, 503.

Stuhrmann H.B. and Kirste R.G., 1967, Z. Phys. Chem. Frankfurt, 56, 333.

Stuhrmann, H.B., 1970, Acta Cryst. A26, 297.

Stuhrmann, H.B., 1978, Quart. Revs. Biophys., 11, 71.

Stuhrmann, H.B., 1980, Acta Cryst., A36,996.

Stuhrmann, H.B., 1981a, Quart. Revs. Biophys. (in press)

Stuhrmann, H.B., 1981b, Kristallographia (in press)

Stuhrmann, H.B., 1981c, Makromol. Chem. (in press)

Stuhrmann, H.B. and Gabriel, A. ,1981, J. Appl. Cryst. (in press)

Stuhrmann, H.B. and Notbohm, H., 1981, Proc. Natl. Acad. Sci. USA (in press)

Takagi, S., Ishida, K. and Ohtsuka, A., 1978, XIth Int. Congr. Crystallogr. Abstract 11.2-18, pp. S254, Warsaw.

Tanner, B.K., Safa, M., Midgley, D. and Bordas, J., 1976, J. Magn. Magn. Mater., 7, 337.

Tanner, B.K., Midgley, D. and Safa, M., 1977, J. Appl. Cryst., 10, 281

Tardieu, A., Luzzati, V. and Reman, F.C., 1973, J. Mol. Biol., 75, 711

Tchoubar, D., Rousseaux, F. Pons, C.H. and Lemonnier, M., 1978, Nucl. Instrum. Methods, 152, 301.

Templeton, D.H., Templeton, L.K., Phillips, J.K.

and Hodgson, K.O. , 1980a, Acta Cryst. A36, 436

Templeton, L.K., Templeton, D.H. and Phizackerley, R.P., 1980b, J. Amer. Chem. Soc. 102, 1185.

Thomson, J.J. and Thomson, G.P., 1933, "Conduction of electricity through gases", 3rd ed. Vol. II p 257 (Cambridge University Press:)

Tuomi, T., Haukkarinen, K. and Rabe, P., 1974, Phys. Stat. Sol.(a) 25, 93.

Vachette, P. , 1980, These de doctorat d' Etat, Universite Louis Pasteur: Strasbourg.

Vainsthein, B.K., 1966, Diffraction of X-rays by chain molecules. (Elsevier Publishing Company: Amsterdam)

Van Hove, L., 1954, Phys. Rev. 95, 249.

Walter, R. and Pohl,R., 1908, Ann. der Phys. 25, 715

Walter, R. and Pohl,R., 1908, Ann. der Phys. 29, 331

Warren, B.E., 1969, X-ray diffraction (Addison-Wesley Publishing Co. Inc.: Reading, Massachusetts)

Warren, B.E. and Gingrich,

Webb, N.G., Samson, S., Stroud, R.M., Gamble,R.D. and Baldeschiwieler, J.D. , 1977, J. Appl. Cryst. 10, 104

Wendin,G., 1980, Physica Scripta, 21, 535.

Zachariasen, U.H., 1967, Theory of X-ray
diffraction in crystals, (Dover Publications Inc.:
New York)

Captions for figures.

Figure 1: Geometry of the scattering problem for a linearly polarized incident X-ray beam.

Figure 2: Scattering of a plane wave by two centres. The phase difference is given by 2π(OA - BH)$/\lambda$, where λ is the wavelength of the incident X-rays.

Figure 3: Definition of the scattering vector $\vec{\mathcal{X}}$. The modulus of $\vec{\mathcal{X}}$ equals $2\mathcal{A}\sin\theta$ as indicated in Eq. 10.

Figure 4: The dependence of the atomic scattering factor $f(\mathcal{X})$ on the modulus of the scattering vector for Calcium ($\bullet$) and Zirconium ($\circ$) atoms as calculated from the electron density distributions obtained from the Thomas-Fermi-Dirac statistical model.

Figure 5: The dependence of f' and f" on the wavelength for Caesium determined from diffraction data in the region of the L1 (left), L2 (centre) and L3 (right) absorbtion edges.

Figure 6: The two-dimensional lattice in real space and the corresponding two-dimensional lattice in momentum space. The reciprocal lattice vector $\vec{s}_{hk}$ is perpendicular to the set (hk) of crystallographic planes.

Figure 7: The Ewald construction in a two-dimensional momentum space. The radius of the Ewald circle is equal to $\frac{1}{\lambda}$ and the centre of the circle is at the origin of the incident wavevector $\vec{k}_i$ terminating at the origin 000 of the reciprocal lattice. The Bragg equation is fulfilled for reciprocal lattice points crossed by the circle.

Figure 8: The reciprocal lattice construction illustrating reflexions of a polychromatic beam from a single crystal set for the HHH Bragg reflexions.

Figure 9: Diffraction patterns of powdered $BaTiO_3$ obtained with a monochromatic beam angular scan method (a) and the energy-dispersive method (b).

Figure 10: Illustrative presentation of the integrated intensity P(s) in case of the angular dispersive method(a) and energy-dispersive method (b).

Figure 11: Oscillation photograph of a single crystal of pig pancreatic amylase (Molecular weight 53000) recorded at LURE-DCI (oscillation range: 3°; exposure time: 750s; source: storage ring DCI operated at 1.72 GeV and 180 mA) (courtesy of R. Haser)

Figure 12: Construction showing unique solution for protein phase angle from single isomorphous replacement and anomalous scattering (SIRAS).

Figure 13: Unique solution for protein phase

angle from single isomorphous replacement with Bijvoet pair measurements at two wavelengths.

Figure 14: SR X-ray diffraction patterns of YbH_2 in a diamond anvil cell at (a) atmospheric pressure (orthorhombic phase) and (b) at 282 kbar (h.c.p.) recorded in 500 s at DORIS (Olsen et al. 1981).

Figure 15: Principle of the experiment designed for the study of magnetic scattering in zinc spinel (courtesy of F. de Bergevin)

Figure 16: Principle of the white beam topography technique (transmission geometry)

Figure 17: Fixed phase stroboscopic X-ray topograph (a) of a Fe 3.5%Si single crystal submitted to a sinusoidal magnetic field (f = 77Hz, amplitude 12 Oe) applied along the vertical direction.
The topograph was recorded with a double axis

spectrometer at LURE, working in the (+,+) setting. A mechanical stroboscope was inserted between the first (Ge[110] crystal and the sample. The X-rays only reached the FeSi crystal when the field was maximum as indicated by the arrow in (b): fixed phase stroboscopy.
White horizontal lines are (110) $90°$ magnetic domain walls. Under the influence of the periodic applied field the wall indicated by the dotted line oscillates from right to left at the field frequency. A and B are the extreme positions of the wall segment JJ'. The oscillation induces small displacements of the horizontal $90°$ walls. For the present phase setting, the oscillation of the wall (dotted line) induces an instability of the $90°$ (110) wall segment between J and D, which is revealed as a broadening of the wall contrast on the right of the dislocation D. The topograph thus provides direct evidence for the interaction of a dislocation and a wall moving under the action of a periodic magnetic field.
(Scale mark: 200 μm, g is normal to the reflecting planes)

Figure 18: X-ray interferometer used by Bonse et

al. (1980). In: interferometer, Mo: monochromator, S: sample, P: phase shifter, SC: scintillation counters, SSD: solid state detector. TV: X-ray television camera for imaging fringe patterns during alignment.(Bonse et al., 1980)

Figure 19: (a) The total intensity (measured by means of energy dispersive diffraction and corrected for primary spectrum, absorption and polarization) as function of the scattering vector. (b) The net liquid structure of Mercury at 25°C and 1 atm. (After Prober and Schultz, 1975)

Figure 20: Variation of the radius of gyration of a ferritin solution in the region of the iron absorbtion edge. (After Stuhrmann 1980)

Figure 21: Time course of the scattering pattern of a solution of tubulin during successive temperature jumps from 4°C to 37°C (H) and reverse (L). For details see text.(After Mandelkow et al. 1980).Time resolution: 15s.

Figure 22: Time course of the difference scattering pattern of a solution of the enzyme ATC-ase during dissociation under the influence of mercurials. The curves were obtained by subtracting the scattering pattern of the final state from the pattern in each time frame. For details see text.

Figure 23: Meridional diffraction pattern of a frog Sartorius muscle showing the orders of the sarcomere length, approximately 50000 Å.

Figure 24: Scattering pattern of pure Al (left) and of an Al-Zn 6% alloy (right). Counting time using a linear position sensitive detector: 100s. (After Haudon et al. 1979)

Figure 25: Scattering pattern of a ferrite ferrofluid with (.....) and without (xxxxxx) magnetic field parallel to the scattering vector. (After Anthore et al. 1979).

Figure 26: Time course of the scattering power of a sample of polyethylene terephtalate during crystallization at different temperatures. (After Elsner et al. 1980).

Figure 27: Evolution of the meridional scattering pattern of a single fibre of rat tail tendon collagen upon drying.

Figure 28: Diffraction pattern of native beef cornea.

Figure 29: Diffraction pattern of a frog sartorius muscle. Note the layer line pattern and the stong meridional 143 Å reflection indicated by the arrow, corresponding to the regular arrangement of the cross-bridges. (Courtesy of H.E. Huxley)

Figure 30: Time course of 143 Å reflexion in the diffraction pattern of frog sartorius muscle during an isometric contraction. The insert shows the tension (continuous curve) and the length of the muscle (dotted line) during the experiment. Time resolution: 1msec.

Figure 31: Time course of the intensities during a phase transition achieved by a temperature jump in an egg lecithin/water system. Note that the intensities are on a logarithmic scale.Time in milliseconds.

Figure 32: Top view of the Risø triple axis spectrometer at HASYLAB showing the monochromator (1), the sample (2) and the analyzer (3) axes. L1, L2 and L3 are levelling screws on the base plate. (Als-Nielsen, 1981)

Figure 33: Diffraction pattern from the (1,0) peak of a two-dimensional "powder" of noble gas physisorbed on a graphite substrate. For Krypton the structure may be in registry with the graphite honeycomb lattice (●) and the sharp cut-off on the

low-wavevector side corresponds to the coherence
length of the substrate (2000 Å). At lower
temperatures (C) there are more Kr atoms than
honeycomb sites and the diffraction peak is
significantly broadened. For Argon the structure
is incommensurate at all fillings and temperatures
with a relatively sharp peak corresponding to a
coherence length of 750 Å. (Als-Nielsen, 1981)

Fig. 1

Fig. 2

Fig. 3

Fig. 4

Fig. 5

$$\vec{a}_1\vec{a}_1^*=2\pi \qquad \vec{a}_1\vec{a}_2^*=0$$
$$\vec{a}_2\vec{a}_2^*=2\pi \qquad \vec{a}_2\vec{a}_1^*=0$$

Real space
$$\vec{p}=p_1\vec{a}_1+p_2\vec{a}_2$$

$$\vec{s}_{HK}=H\vec{a}_1^*+K\vec{a}_2^*$$
Ex.: $\vec{s}_{23}=2\vec{a}_1^*+3\vec{a}_2^*$
$$s_{hk}=2\pi/d_{hk}$$

Momentum space

Fig. 6

Fig. 8

$\vec{\varkappa} = \vec{k}_f - \vec{k}_i$

$|\vec{k}_i| = |\vec{k}_f| = k_i$

Ewald "circle"

$\vec{k}'_f$

H'K'L'

θ θ

2θ

$\vec{k}_f$

$\vec{k}_i$

HKL

$\vec{\varkappa} = \vec{S}_{HKL}$

000

Fig. 7

Fig. 9a

Fig. 9b

a)

b)

Fig. 10

Fig. 11

Fig. 12

Fig. 13
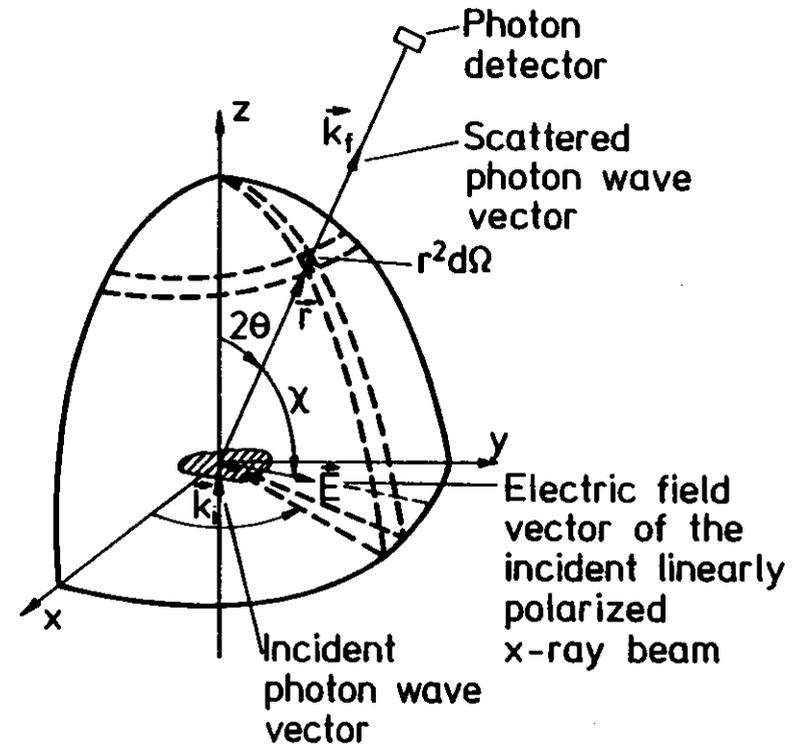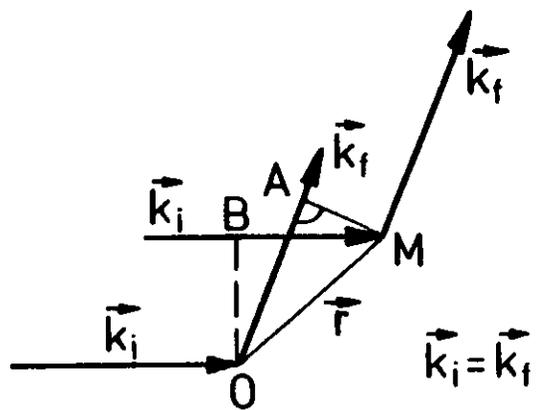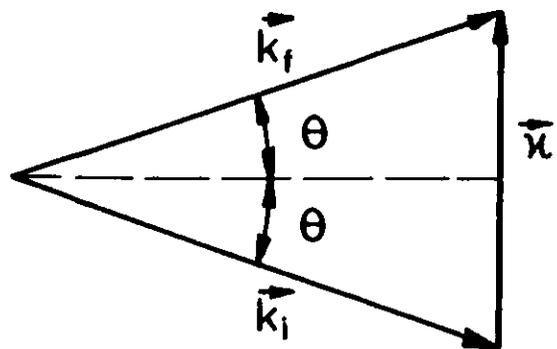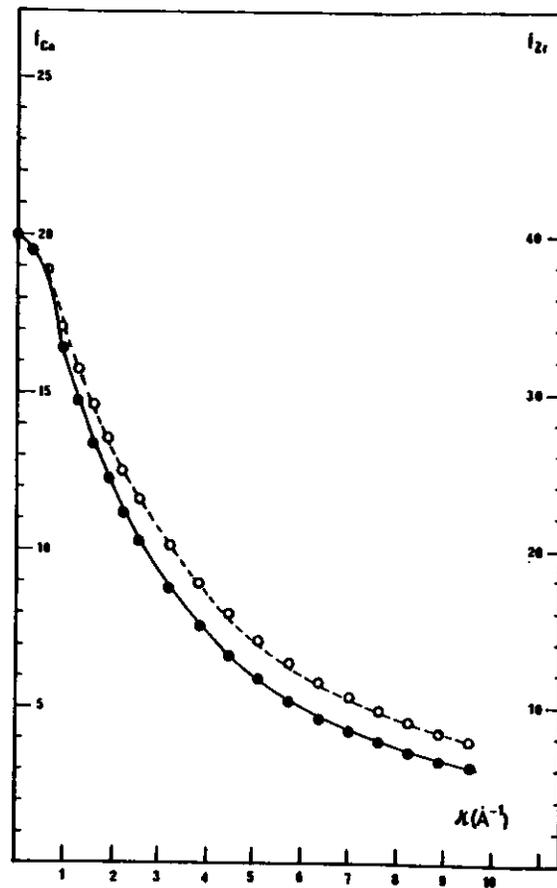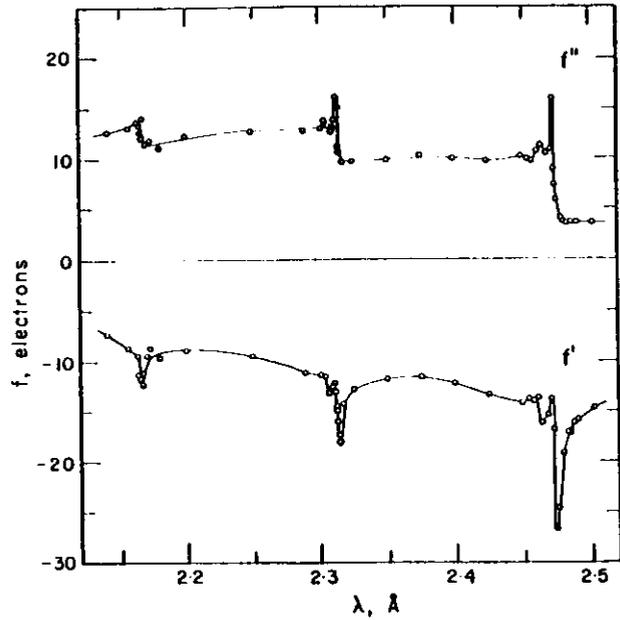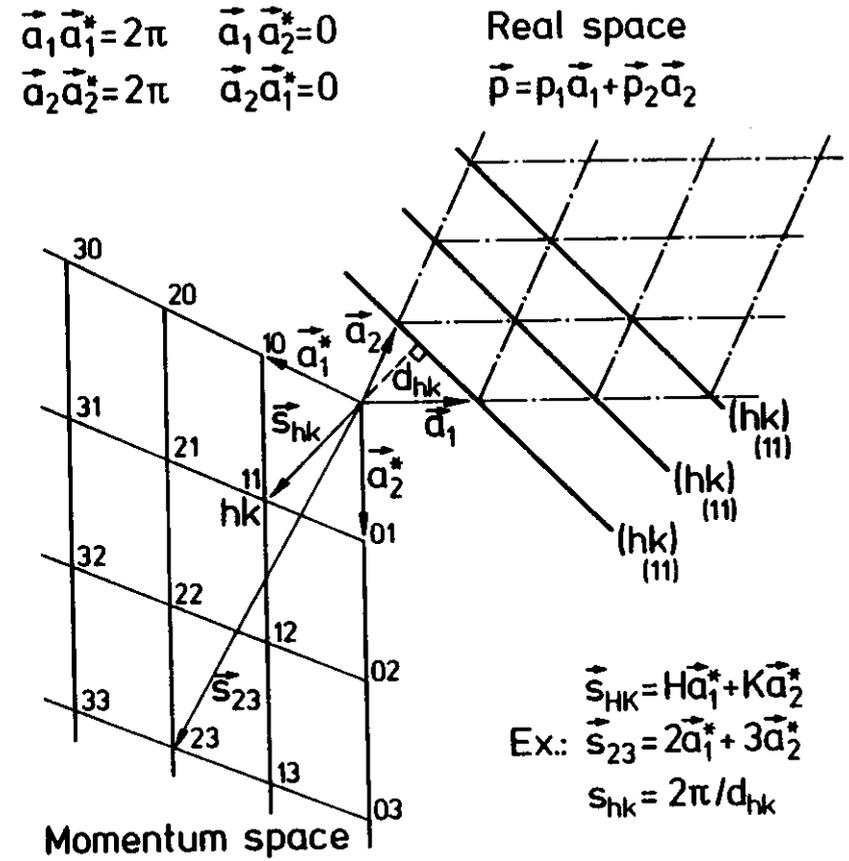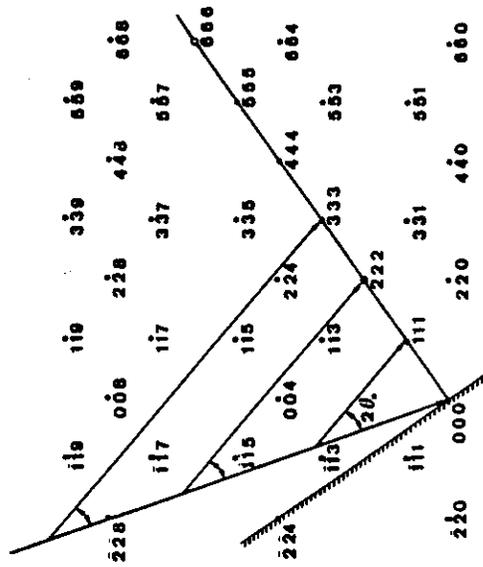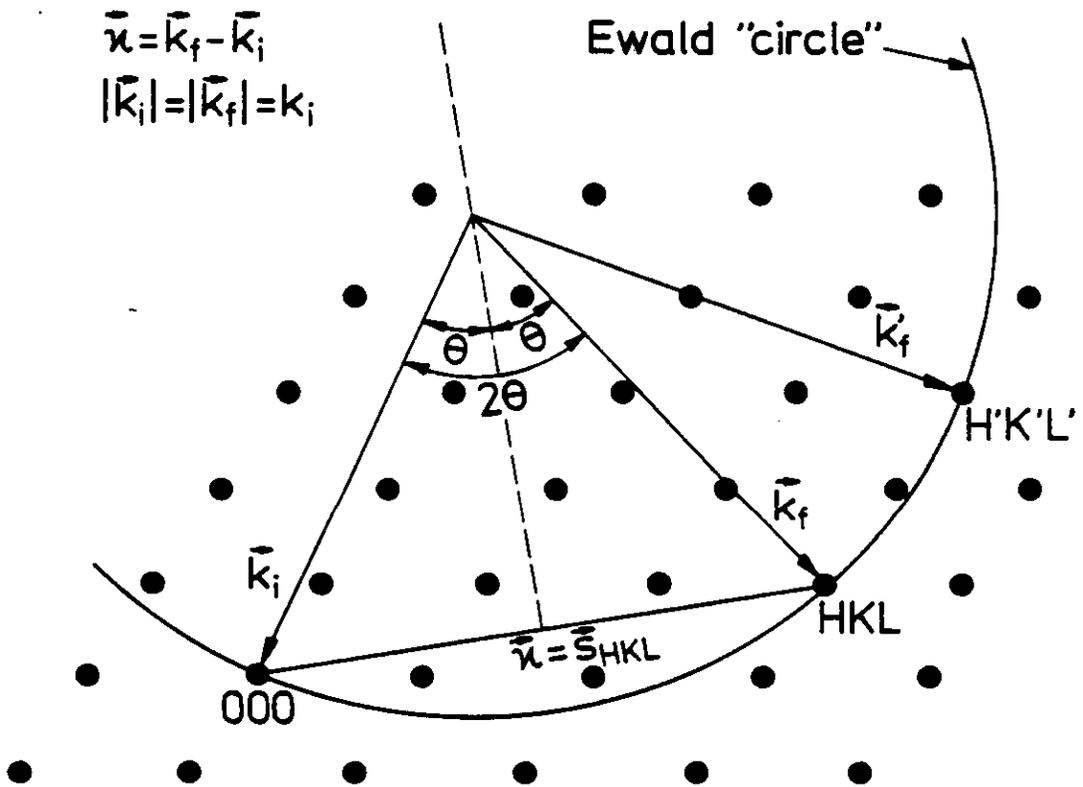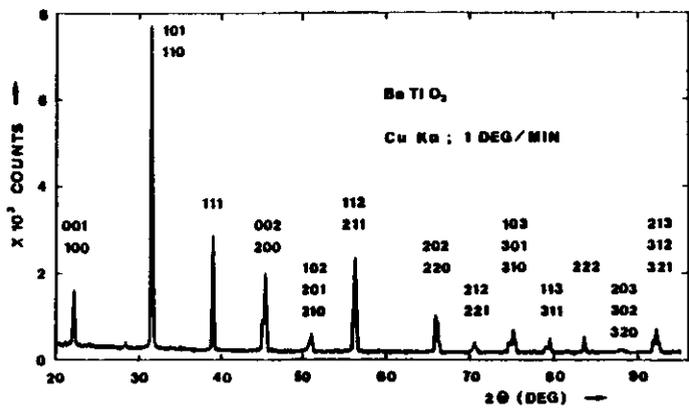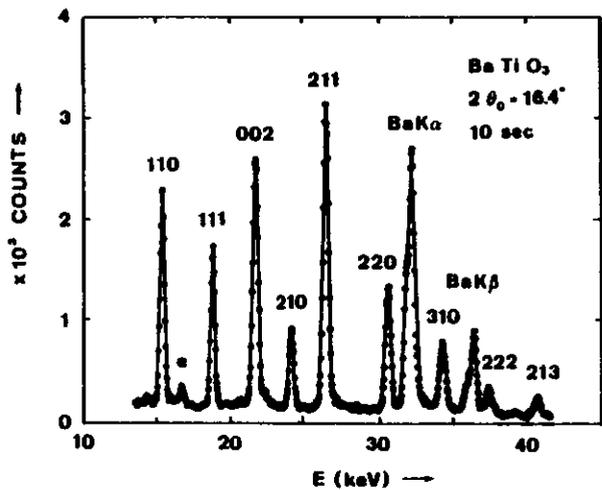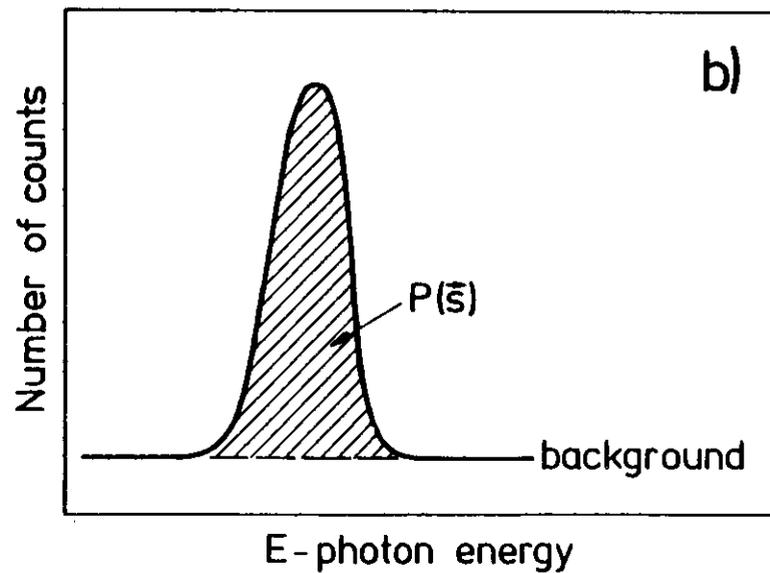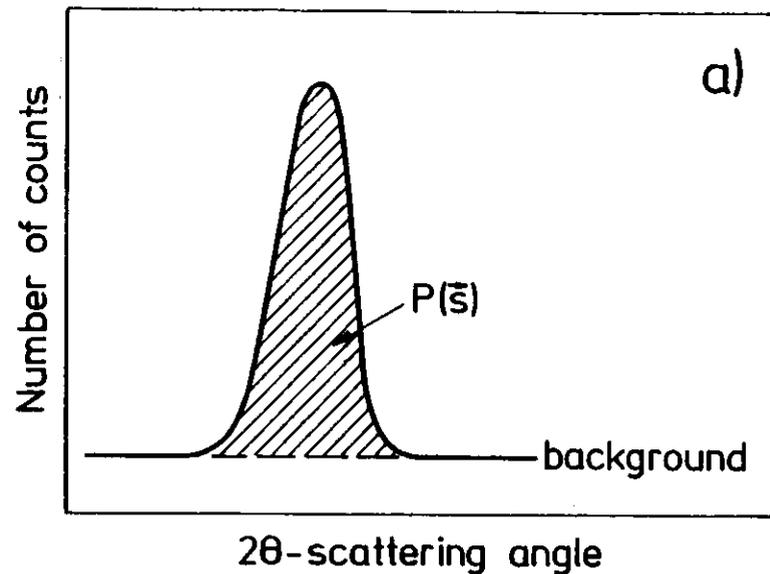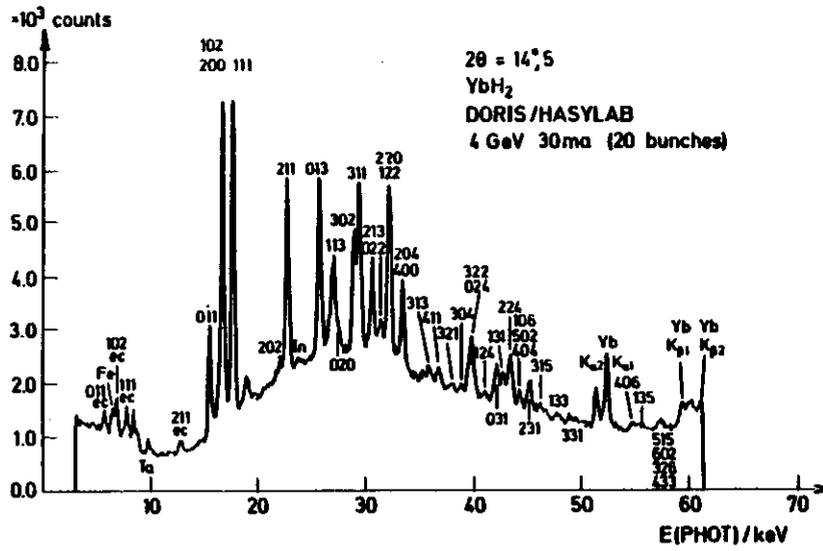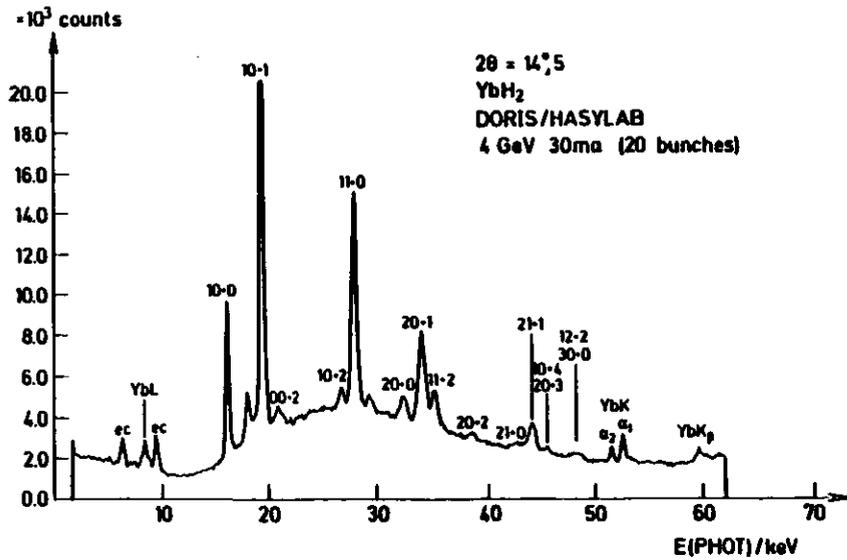
Fig. 14a

Fig. 14b

Fig. 15

Fig. 16

Fig. 17

Total Intensity (arbitrary units)

$s = 4\pi \sin\theta/\lambda$ (Å^{-1})

Fig. 19a

$4\pi r^2 \rho_o [g(r)-1]$ (Å^{-1})

r (Å)

Fig. 19b

DORIS

Mo

In

θ_1

θ_2

S

P

SC

SC

SSD

TV
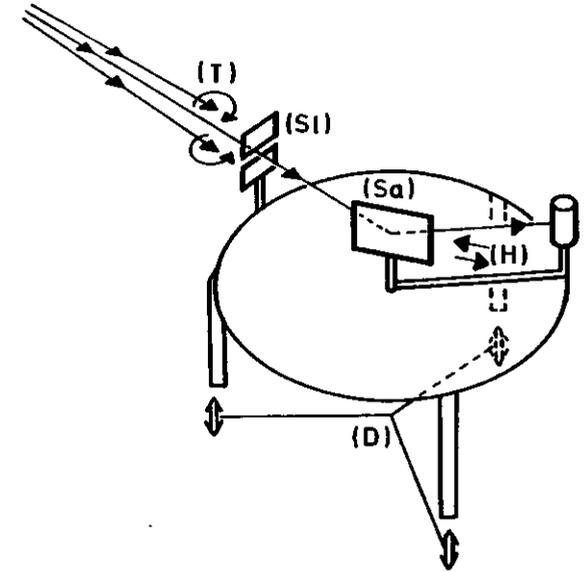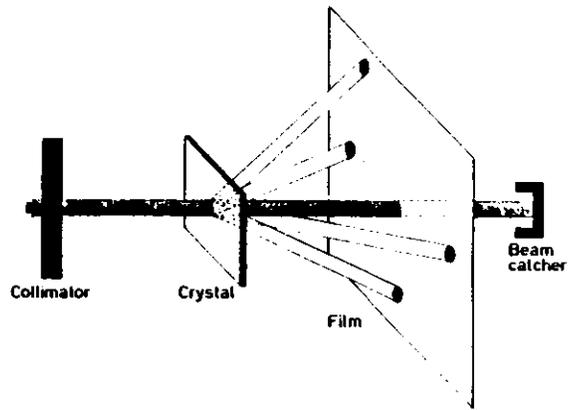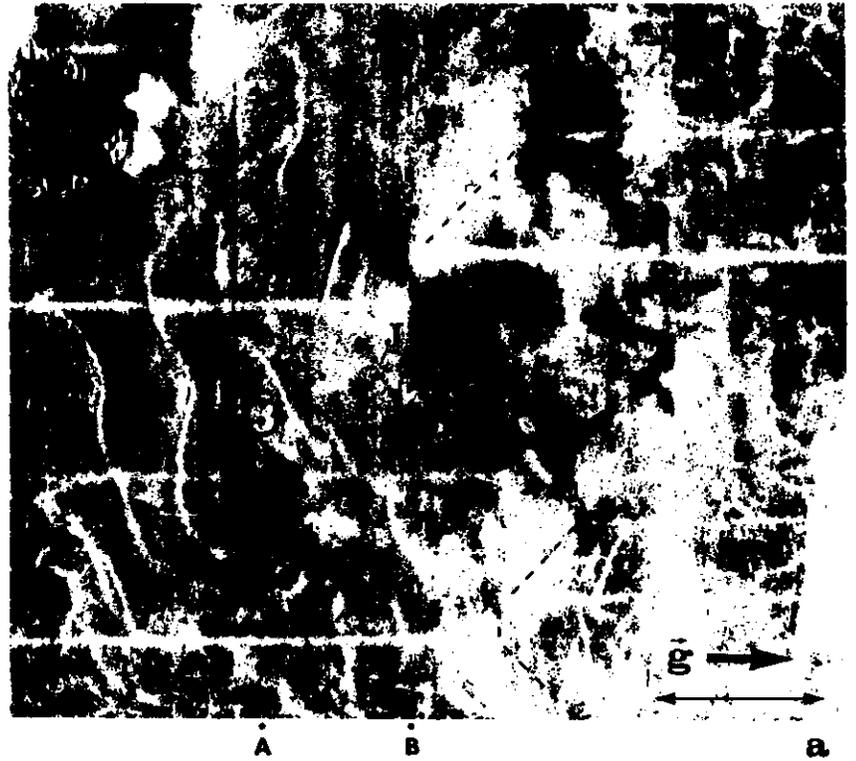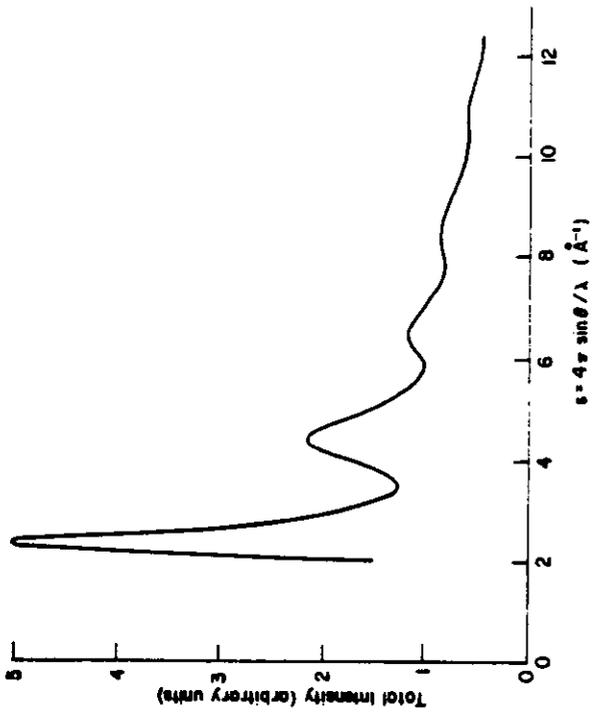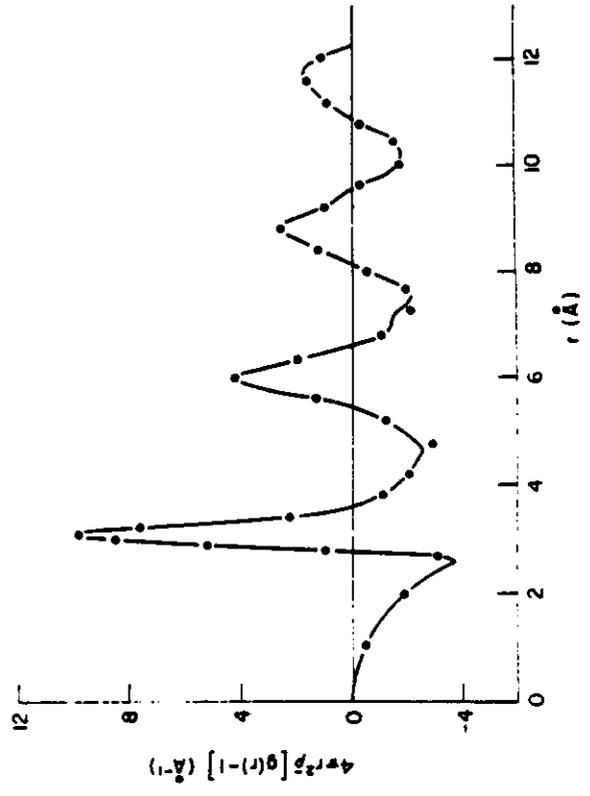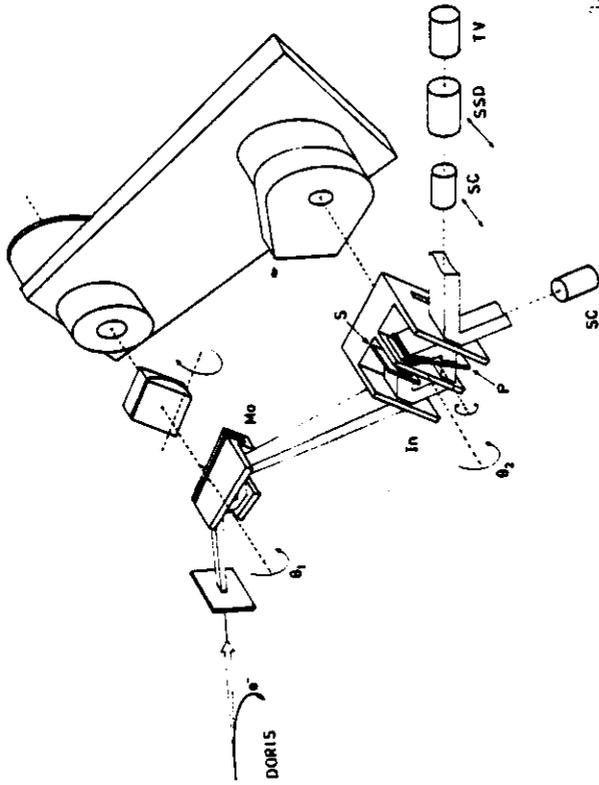
Fig. 18
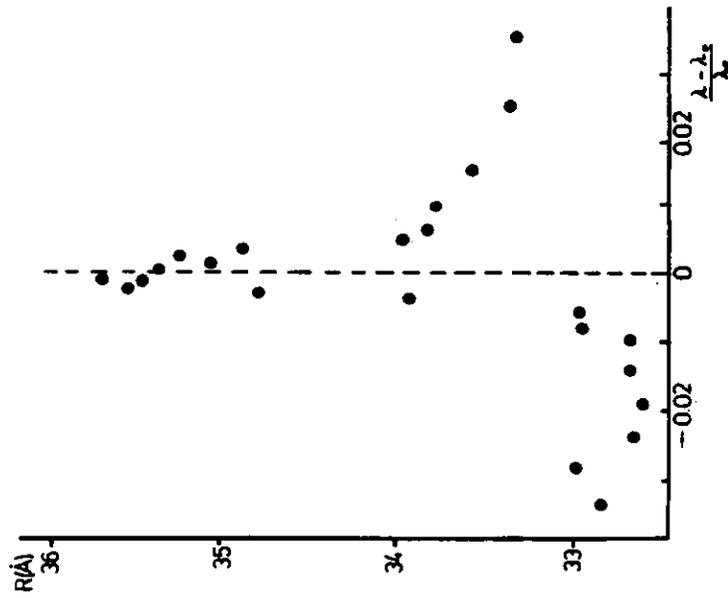
Fig. 21

Fig. 20
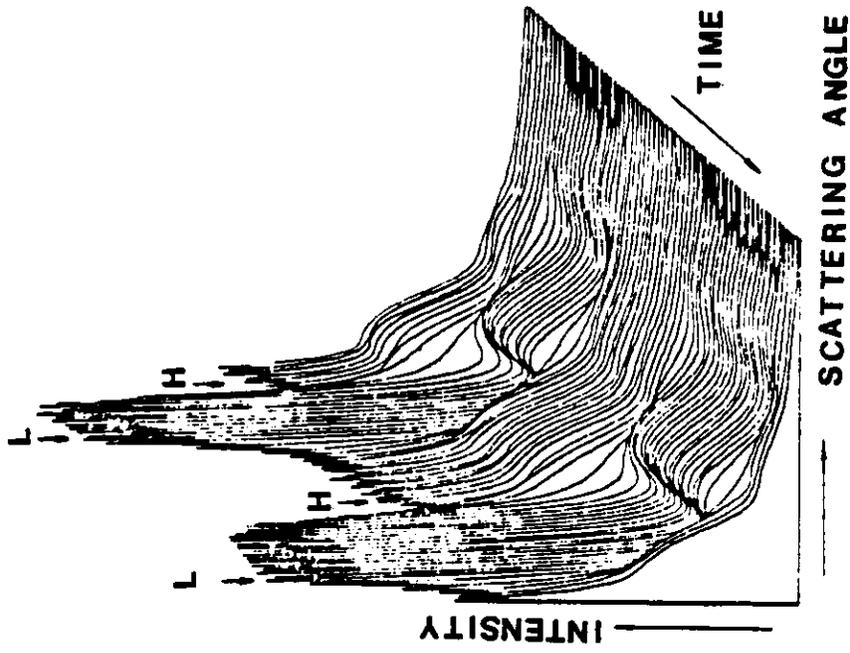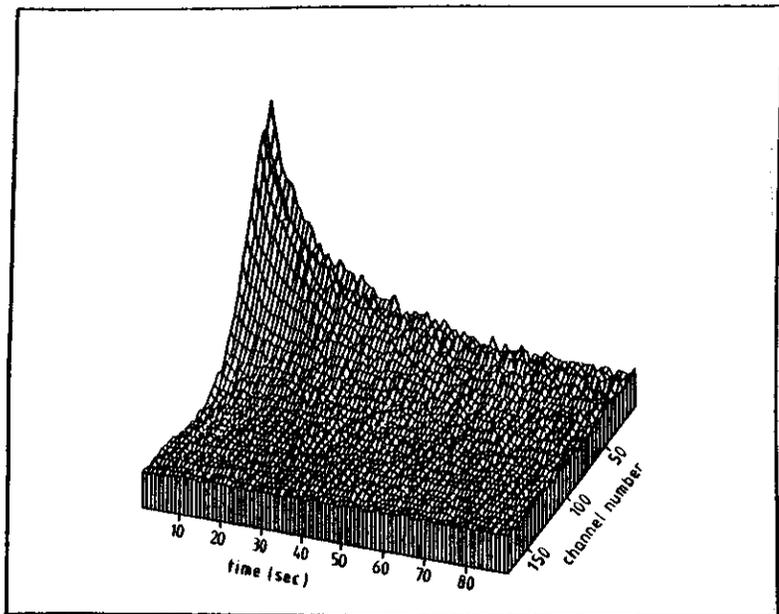
Fig. 22
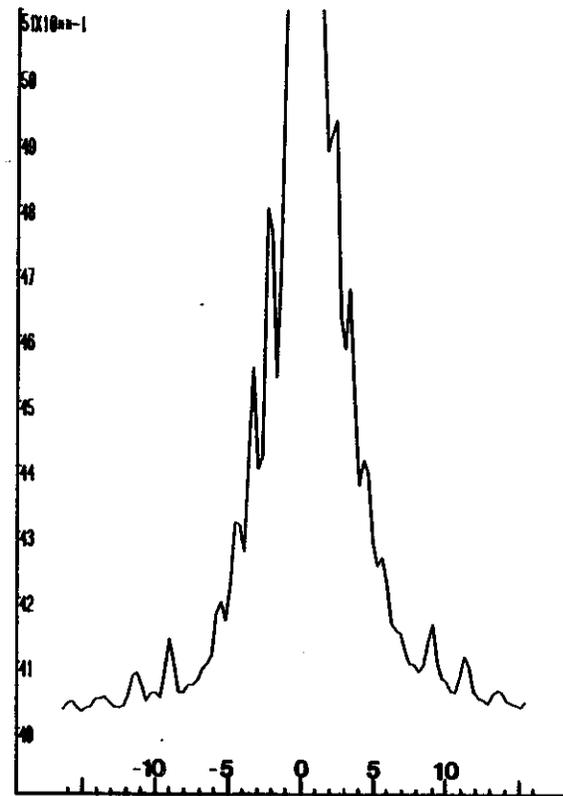
Fig. 23
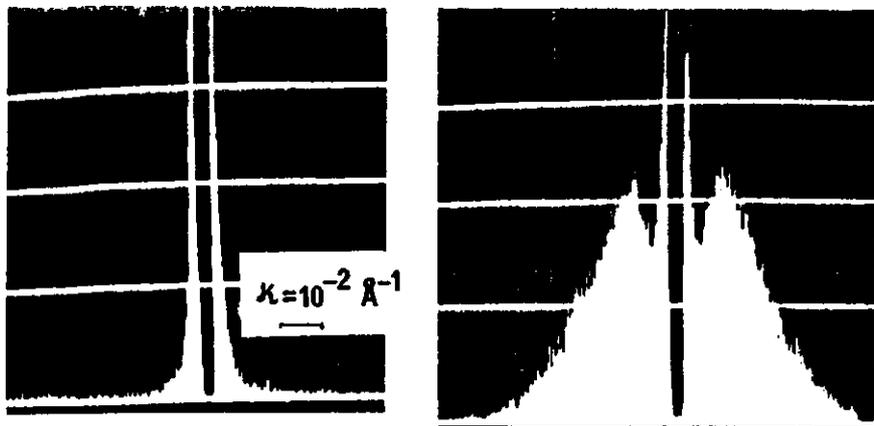
Fig. 24
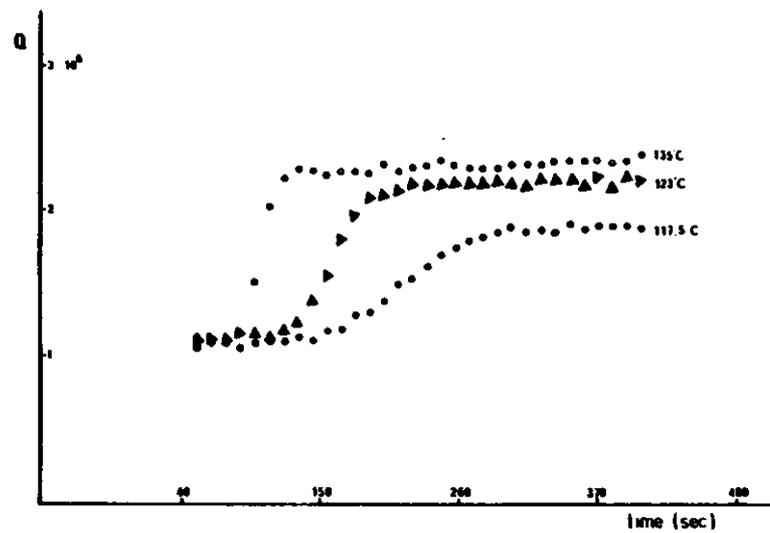

Fig. 26
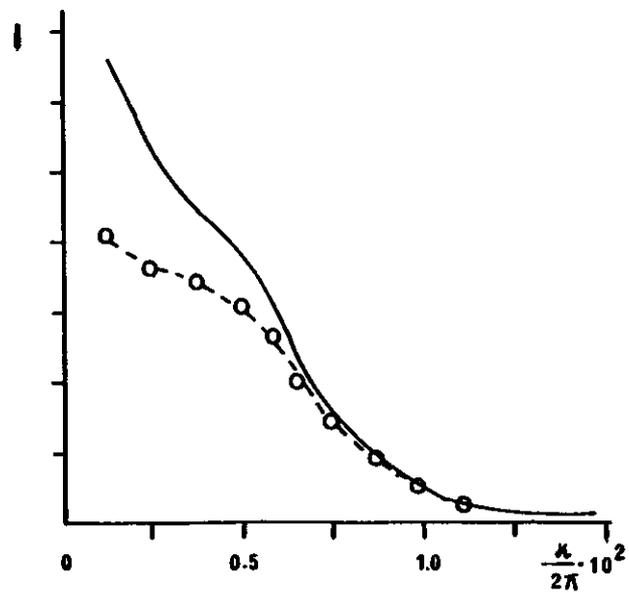
Fig. 25
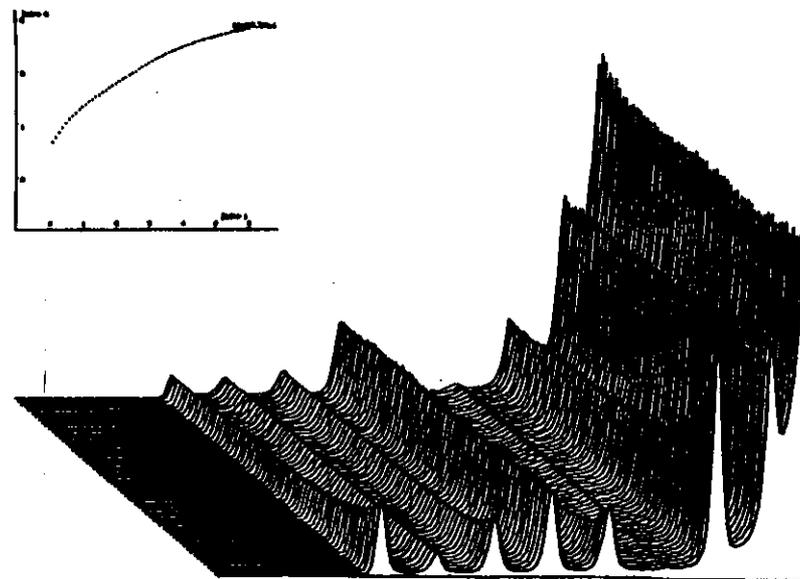
Fig. 27

Fig. 28

Fig. 29

Fig. 30

Fig. 31

Fig. 32

Fig. 33